(3) Occurrence

In addition to the Morphology and Size of manganese nodules, the following characteristics of occurrence were recognized.

① Crushed manganese nodules occur at about half of the sampling points. They occur abundantly in the eastern sea off the Line Islands.

② Sizes are lacking in uniformity and various sizes of manganese nodules occur in the same areas.

③ Embedded rate*1 is high. Embedded nodules were recognized at 78 sampling points and the embedded rate marks 79% of the total. The average embedded rate is 80%. Embedded rate in the western sea off the Line Islands is higher than that in the eastern sea.

	Embedded Rate
Western sea off the Line Islands	87%
Eastern sea off the Line Islands	73%

Typical occurrence is shown in Figure 3-5-4.

2) Abundance

Abundance Map of manganese nodules is shown in Annexed Figure 10. The average value of abundance is comparatively low in the survey area, but parts of the eastern sea of the Line Islands have zones with higher values.

Characteristics of abundance in this sea area are as follows:

① Average abundance of all the sampling stations (33 stations) is 4.37 kg/m^2, a low value. According to the Figure 3-5-5, 68% of the total sampling points are barren with abundance of less than 2.5 kg/m^2.

② Zones with high abundance of over 10 kg/m^2 occur in the eastern part of the survey area, but the rate of occurrence marks only 8%. The highest abundance of 21.13 kg/m^2 occurs in the eastern sea of the survey area.

③ Zones with medium abundance of 5 kg/m^2 to 10 kg/m^2 are found here and there.

---

*1 The definition of the Embedded rate is as follows:

$$\left(1 - \frac{\text{population at sea bottom}}{\text{population on board}}\right) \times 100$$

89S1147FG03 (Sea bottom)
Depth: 4,790m
Massive type, Pebble type

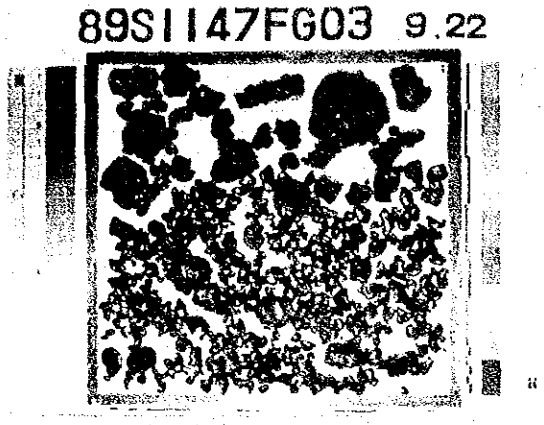

Same as left (Sample collected)
Calc-siliceous Clay
Abundance 14.61 kg/m^2

89S1147FG01 (Sea bottom)
Depth: 4,810m
Plate type, Pebble type

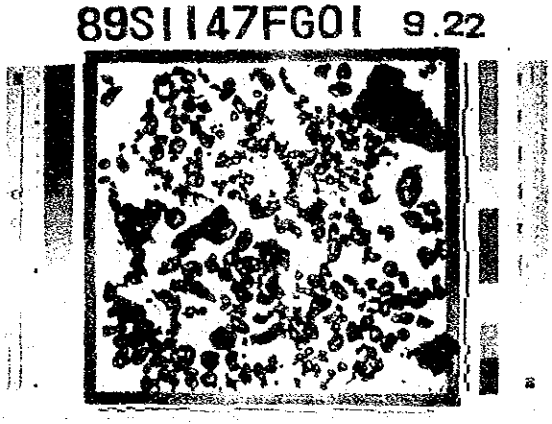

Same as left (Sample collected)
Silic-calcareous Clay
Abundance 4.70 kg/m^2

89S0841FG02 (Sea bottom)
Depth: 5,010m
Crust type

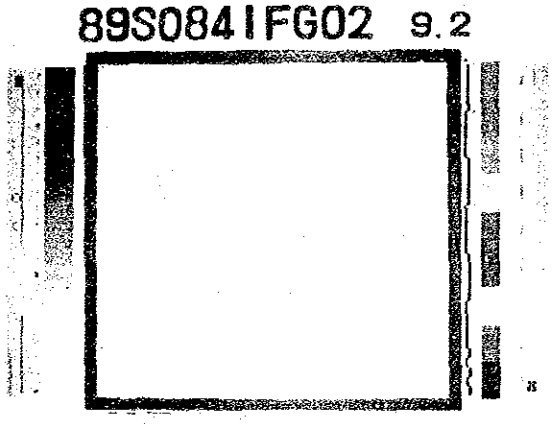

Same as left (Sample collected)
Abundance ————

Figure 3-5-4 Photos of Sea Bottom and Samples Collected (1)

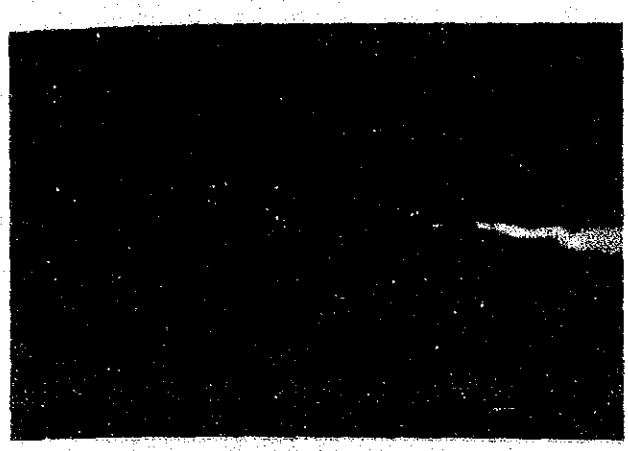

89S0946FG01 (Sea bottom)
Depth: 5,025m
Pebble type, Pebble thin type

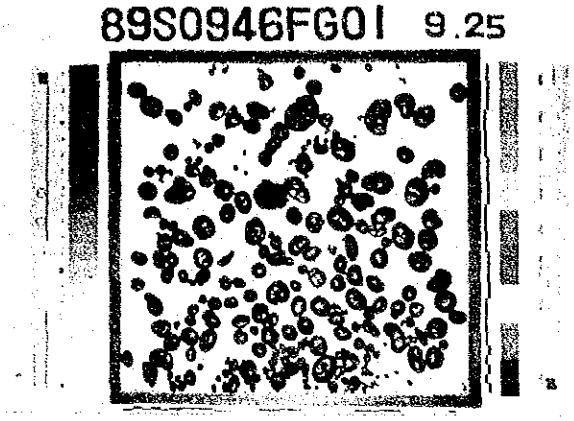

Same as left (Sample collected)
Brown Clay
Abundance 6.19 kg/m^2

89S0947FG03 (Sea bottom)
Depth: 4,815m
Spheroidal type, Pebble thin type

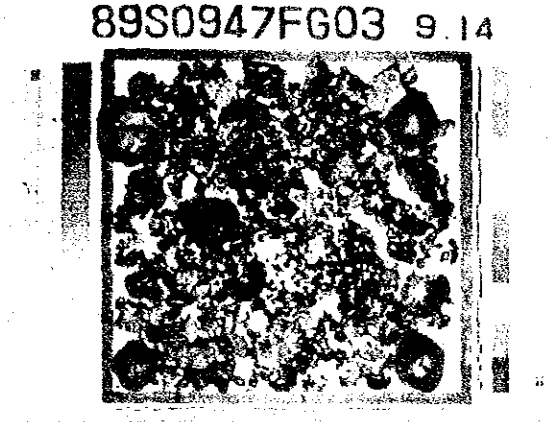

Same as left (Sample collected)
Silic-calcareous ooze
Abundance 20.90 kg/m^2

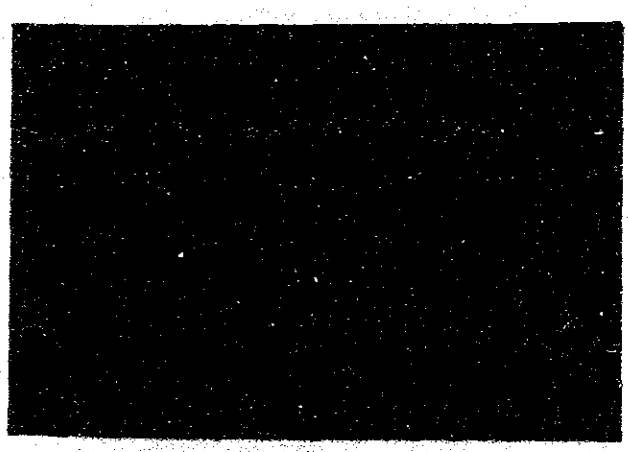

89S0742FG03 (Sea bottom)
Depth: 5,065m
Ellipsoidal type

Same as left (Sample collected)
Brown Clay
Abundance 2.29 kg/m^2

Figure 3-5-4 Photos of Sea Bottom and Samples Collected (2)

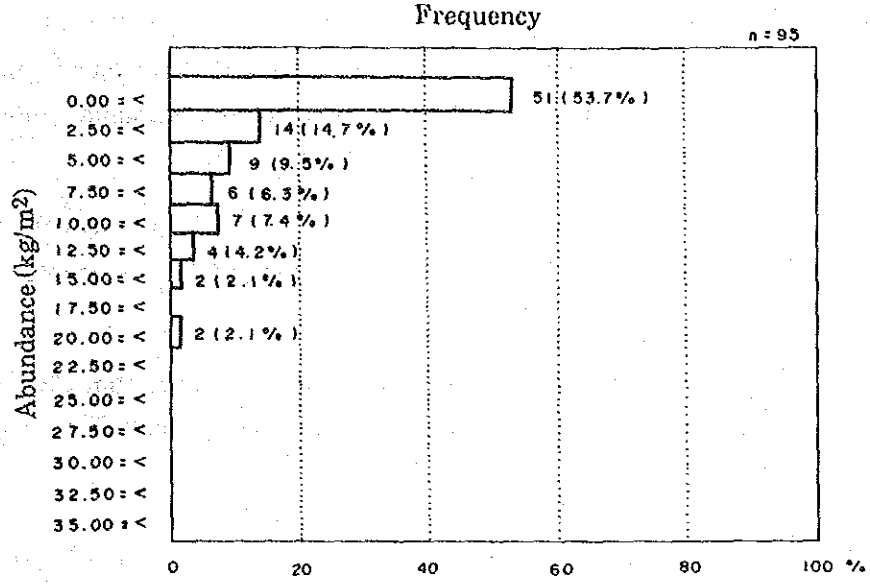

Figure 3-5-5 Relation between Abundance and Frequency (Sampling Points)

④ Different average abundance is recognized between the eastern seas and the western seas off the Line Islands. The eastern sea area has higher abundance.

Western sea off the Line Islands	2.94 kg/m^2 (60 sampling points)
Eastern sea off the Line Islands	6.56 kg/m^2 (39 sampling points)

⑤ There is a certain relation among high abundance, depth and topography. The following differences are noticed between the eastern sea and the western sea off the Line Islands;

(a) Seamounts at the depth of 4,700~5,100m of the eastern sea area of the Line Islands show the abundance of over 10 kg/m^2.

(b) Favorable zones are recognized in the western sea area off the Line Islands at a depth of 5,300~5,500m.

⑥ In the eastern sea area off the Line Islands, high abundance of nodules occurs right above and right under the CCD. But in the western area off the Line Islands, high abundance of manganese nodules occurs in the sea areas deeper than the CCD. (Fig. 3-5-6, Fig. 3-5-7)

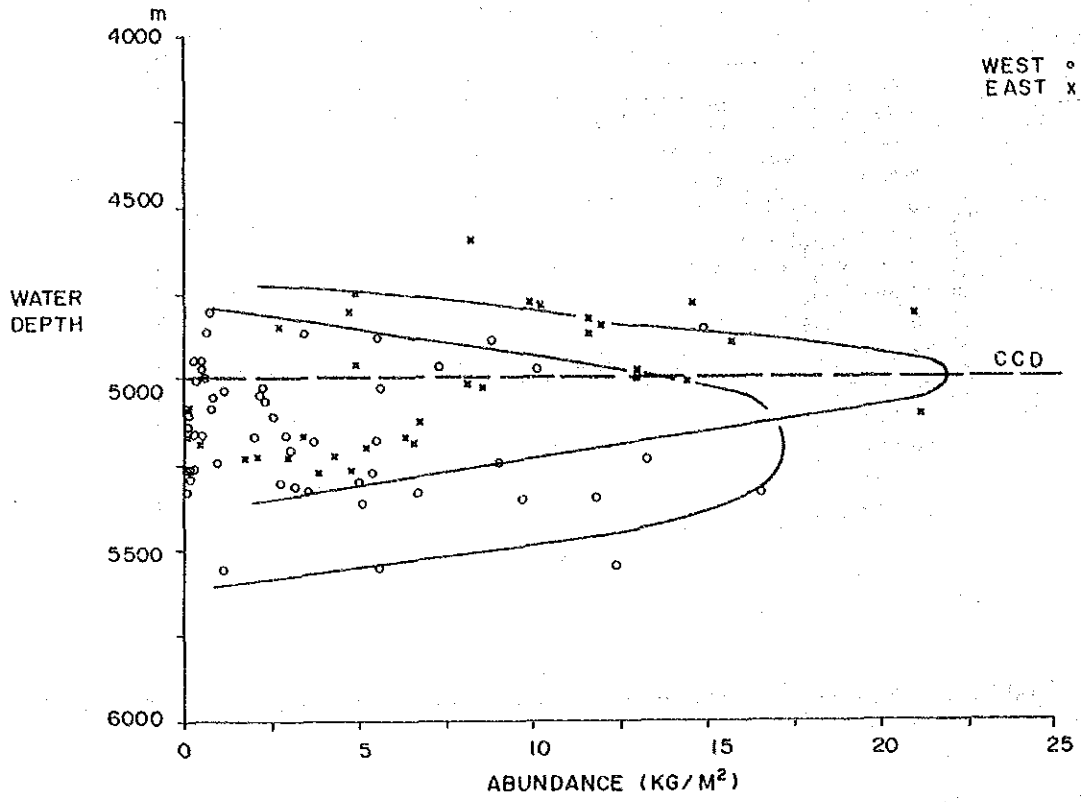

Figure 3-5-6 Relation between Abundance and Water Depth (1)

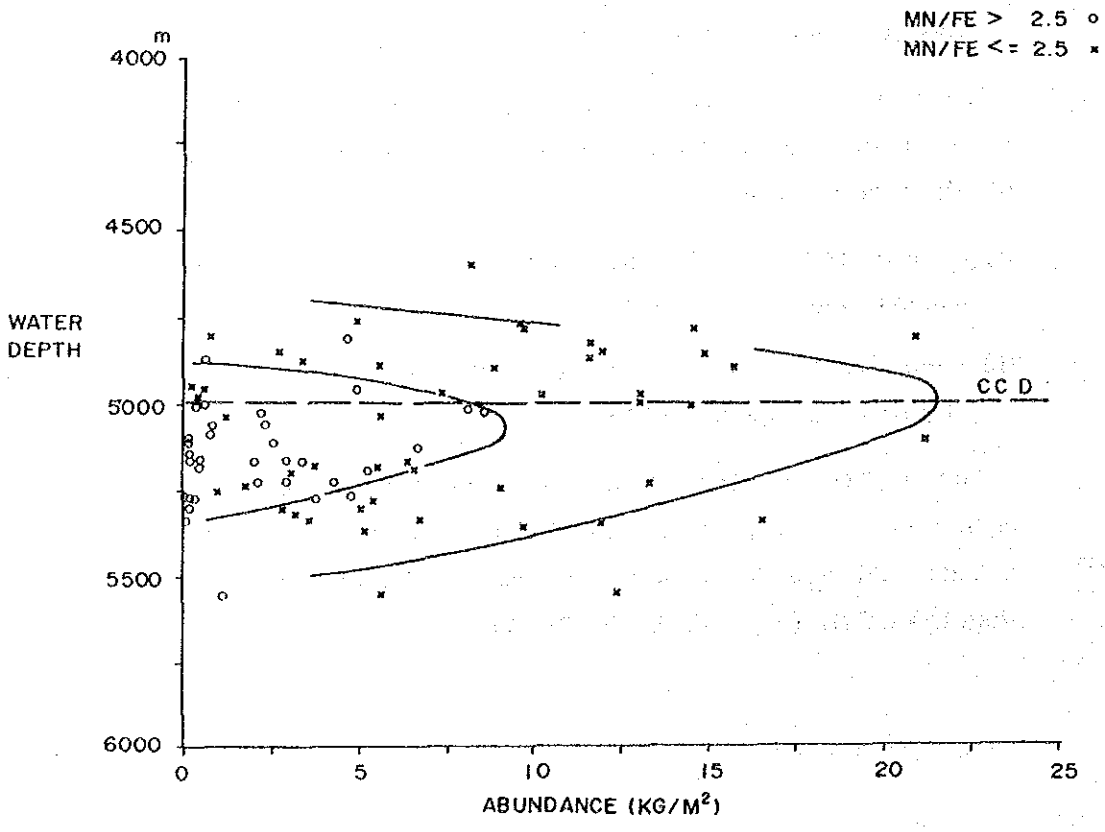

Figure 3-5-7 Relation between Abundance and Water Depth (2)

⑦ The relation between the type of bottom materials and the abundance of manganese nodules shows that the sea areas with calcareous sediments have higher abundance of manganese nodules. (Fig. 3-5-8, Fig. 3-5-9)

	Average abundance
Brown clay	3.72 kg/m^2
Calcareous sediments	7.76 kg/m^2

⑧ The relation between morphology and abundance of manganese nodules shows high abundance of massive and plate types, medium abundance of pebble thin and pebble types, and low abundance of spheroidal type nodules. (Fig. 3-5-10)

3) Chemical Composition

Fluorescent X-ray analysis of five principal components (Ni, Cu, Co, Mn and Fe) of each classified-size was done on board. Representative samples were selected for further analysis of auxiliary components to be done on shore. The results of both analyses on chemical properties of manganese nodules are as follows:

(1) Five principal components and their distribution

Frequency distribution of five principal components is shown in Figure 3-5-11.

Scatter distribution diagrams of two components among five are shown in Figure 3-5-12.

Statistics of average grade are shown in Table 3-5-1.

The average values of Ni, Cu and Co are 0.84%, 0.57% and 0.20% respectively. These values are low with the exception of Co. The average values of Mn and Fe are 20.49% and 9.21% respectively. These average values are the reflection of the grade of pebble-type manganese nodules collected in a large amount.

Grade maps of Ni, Cu, Co, Mn and Fe, are shown in Annexed Figures.

These figures show that the northern part of the survey area has higher than average values of Ni and Cu.

On the other hand, Co grade is high in the western and eastern part of the sea, corresponding to the high abundance zones of the survey sea area.

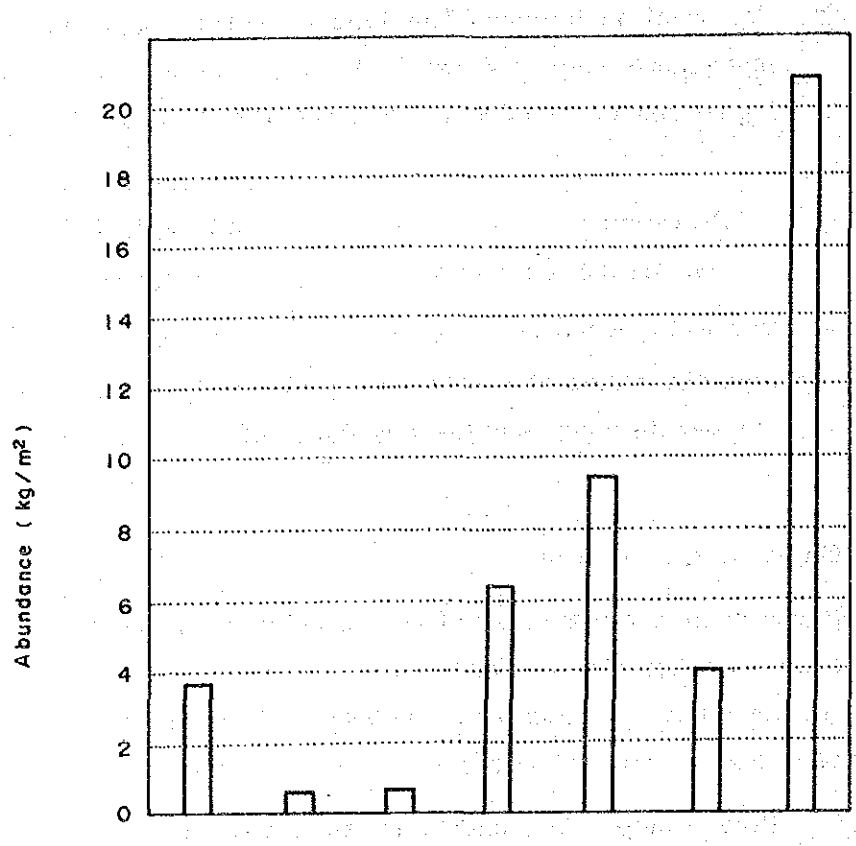

Bottom sediment	BC	SC	CC	SCC	CSC	FO	SCO
Average Abundance (kg/m²)	3.72	0.71	0.73	6.57	9.46	4.08	20.90
Appearance ratio of ≧10kg/m²	11.1	0	0	33.4	57.1	0	100
Standard deviation	4.52	0	0	5.19	4.79	4.08	0
Number of Sample	63	1	1	9	7	2	1

LEGEND

Sediment	BC	Brown clay
	SC	Siliceous clay
	CC	Calcareous clay
	SCC	Silic-calcareous clay
	CSC	Calc-siliceous clay
	FO	Foraminifera ooze
	SCO	Silic-calcareous ooze

Figure 3-5-8 Relation between Bottom Materials and Abundance (1)

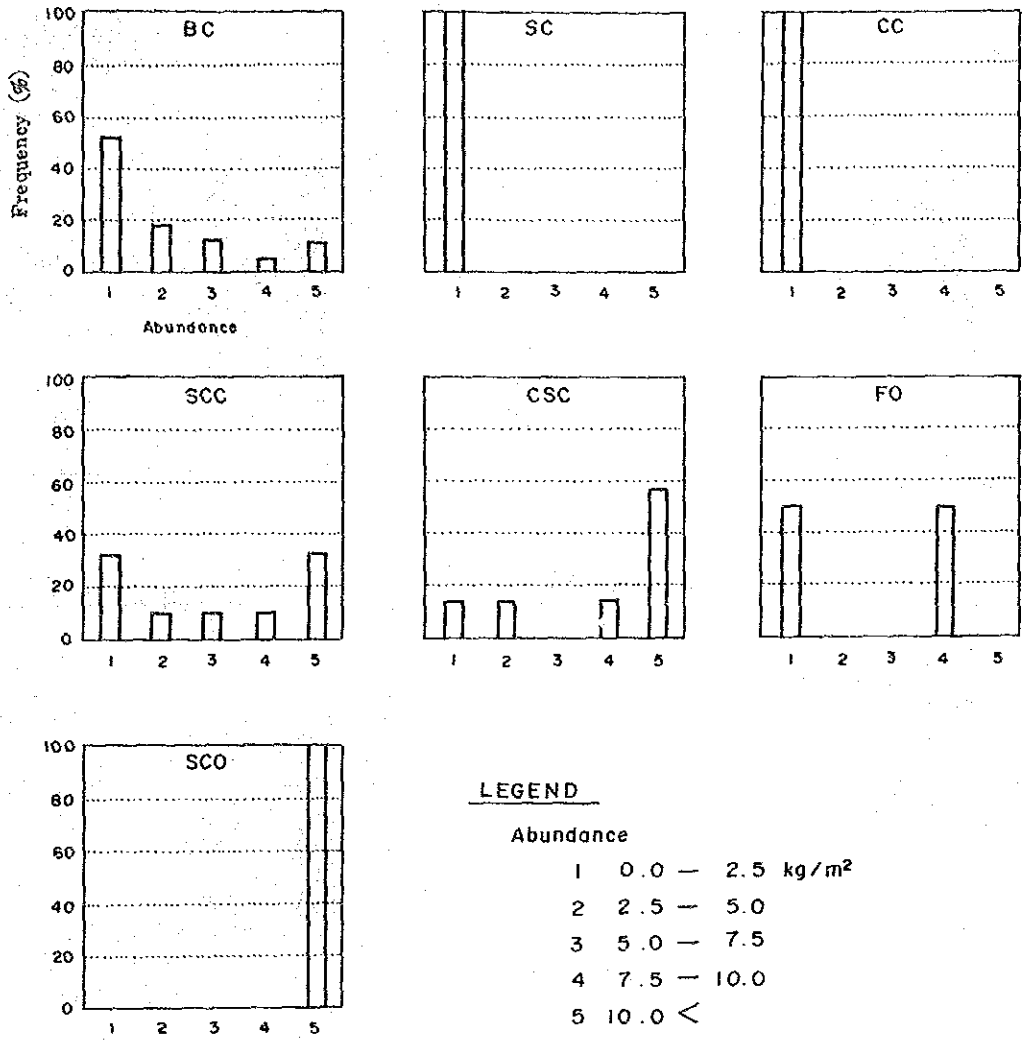

Figure 3-5-9 Relation between Bottom Materials and Abundance (2)

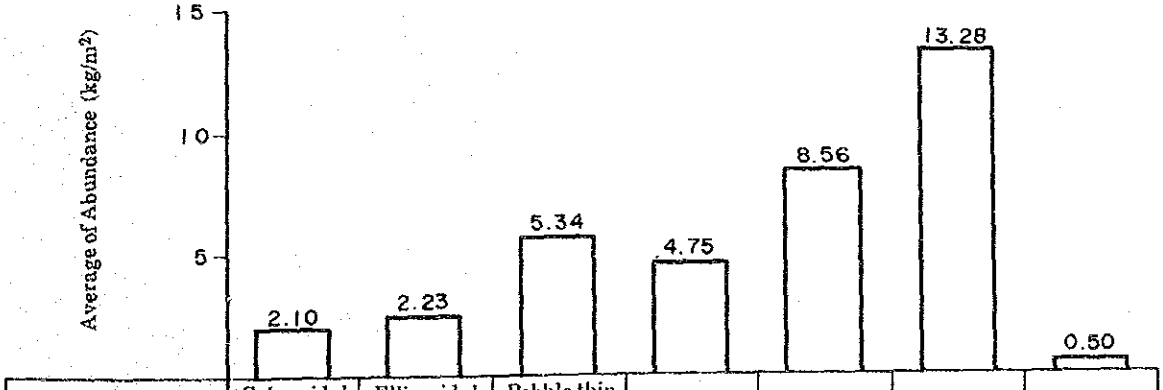

Morphology	Spheroidal type	Ellipsoidal type	Pebble thin type	Pebble type	Massive type	Plate type	Others
Sampling points	15	5	10	41	10	1	1

Figure 3-5-10 Morphology and Average Abundance

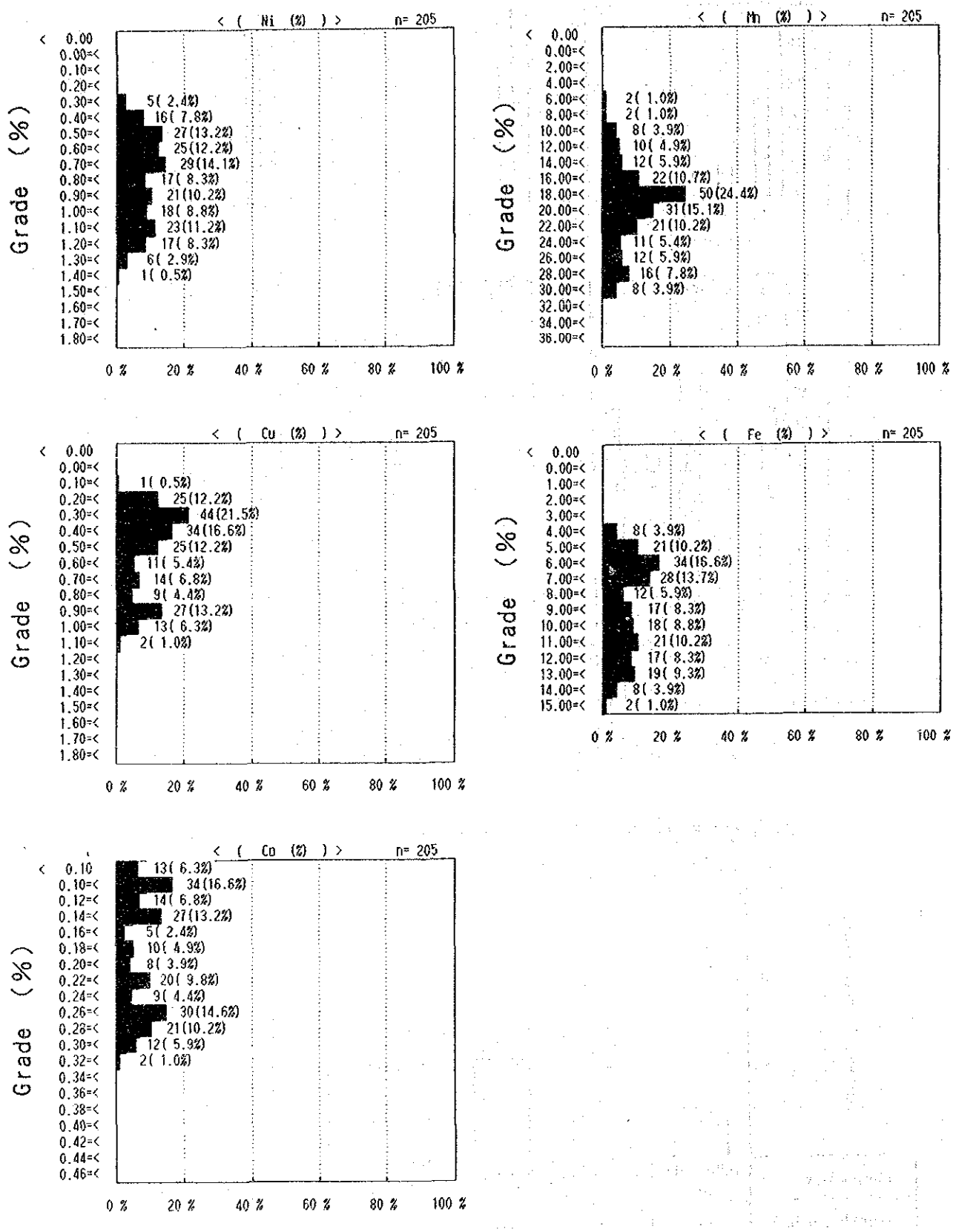

Figure 3-5-11 Frequency Distribution of Five Principal Components

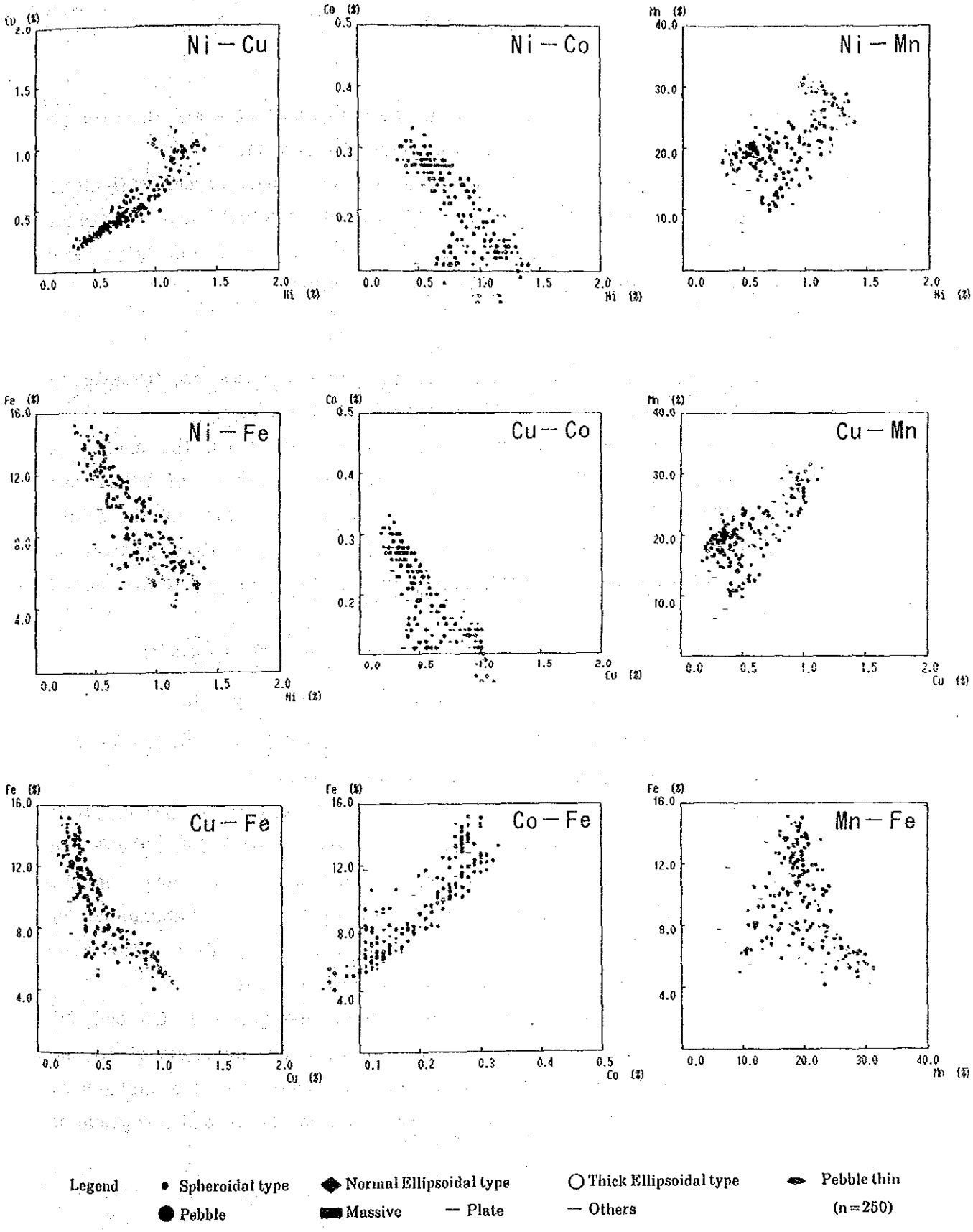

Figure 3-5-12 Scatter Distribution Diagrams between Two Components

Distribution of each component is as follows:

① Ni

The maximum grade of Ni is 1.40%, the minimum 0.33% and the average 0.84%. Grade map of Ni is shown in Annexed Figure 11.

The grade of Ni is high in the northern part of the survey area, particularly in the sea within the enclosures northward of 8°00'S and 148°30'W-151°30'W as well as northward of 7°00'S and 152°30'W-153°30'W. The grade of Ni in these enclosures is higher than 1.00%.

② Cu

The maximum grade of Cu is 1.16%, the minimum 0.18% and the average 0.57%. Grade map of Cu is shown in Annexed Figure 12.

The grade of Cu has similar tendencies to that of Ni, the enclosures northward of 8°00'S and 148°30'W as well as northward of 7°00'S and 152°30'W-153°30'W show high grade but the western part and the south-eastern part of the survey area are low. The sea areas with a grade of Cu over 1.00% occur only sporadically in the northeastern part of the survey area.

The correlation between Ni and Cu is as high as 0.91 (Table 3-5-1).

③ Co

The maximum grade of Co is 0.33%, the minimum 0.04% and the average 0.20%. Grade map of Co is shown in Annexed Figure 13.

There are comparatively high-grade zones of Co with more than 0.25% at the western part of the sea area, in the enclosure of 8°30'S-10°00'S and 153°30'W-154°30'W, and at the eastern part of the sea area, in the enclosure of 8°00'S-9°00'S and 148°30'W-149°30'W. The abundance of manganese nodules in this eastern zone is over 10 kg/m^2, and this zone corresponds to the highest zone in the whole survey area.

According to the Figure 3-5-13 and 3-5-14, the grade of Co and the abundance are in positive correlation, but between the grade of Ni and abundance the correlation is negative. It means that the manganese nodules in area of high abundance have high grade of Co and low grade of Ni.

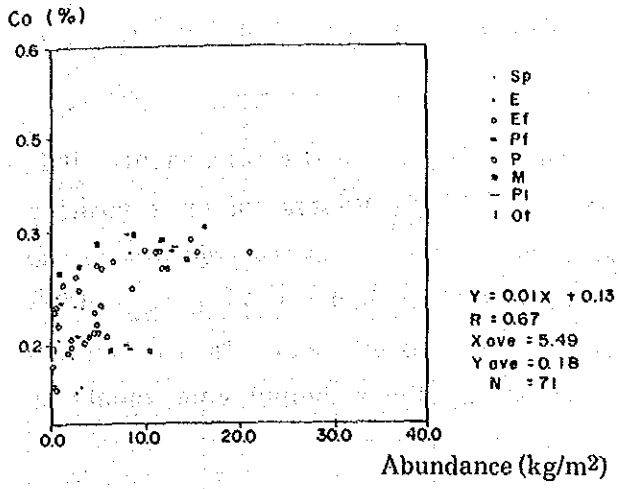

Figure 3-5-13 Abundance — Co Scatter Diagram

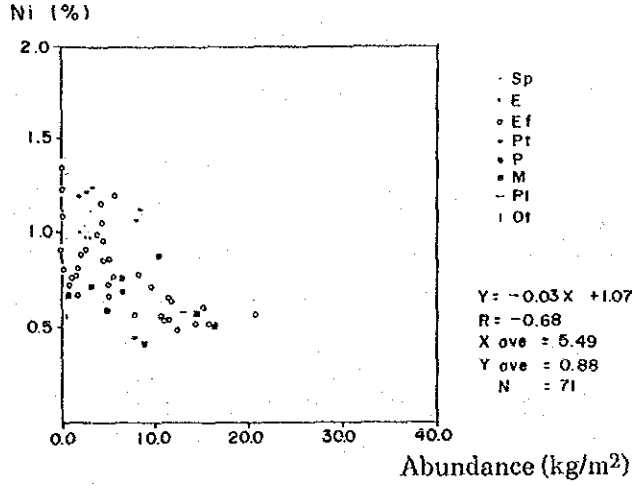

Figure 3-5-14 Abundance — Ni Scatter Diagram

④ Mn and Fe

The maximum grade of Mn is 31.35%, the minimum 6.20% and the average 20.49%. The maximum grade of Fe is 15.07%, the minimum 4.09% and the average 9.21%. The grade of Mn has similar tendency with Ni and Cu, high grade Mn is distributed at the northern and the eastern parts of the survey area.

(2) Grade Characteristics

① Correlation among the components

The Table 3-5-1 shows the correlation coefficients of the components. It is evident that the Ni-Cu-Mn system and the Co-Fe system have positive correlations respectively but the correlation between the two systems is negative. Mn is in positive correlation with Ni and Cu, Fe is in positive correlation with Co, but in negative correlation with Mn. This relationship also exists in the scatter diagrams among the principal components as shown in Figure 3-5-12.

② Grade and Morphology

Table 3-5-2 shows the grade characteristics classified by the shape of manganese nodules. The results are as follows:

(a) Spheroidal and normal ellipsoidal types have similar grade tendencies containing high grade Ni, Cu and Mn but low grade Co and Fe. The ratio of Cu to Ni and Mn to Fe are high.

(b) Pebble, massive and plate types indicate similar grade tendencies containing low grade Ni, Cu and Mn but high grade Co and Fe. The ratio of Cu to Ni and Mn to Fe are low.

(c) Other types are low-grades; the conceivable cause of might be the effect of rock fragments that constitute the core.

Table 3-5-1 Chemical Properties of Manganese Nodules

(n=205)

	Statistics (%)				Correlation Coefficient				
	Average	Standard Deviation	Max.	Min.	Fe	Mn	Co	Cu	Ni
Ni	0.84	0.27	1.40	0.33	−0.85	0.61	−0.75	0.91	1.00
Cu	0.57	0.26	1.16	0.18	−0.85	0.73	−0.84	1.00	
Co	0.20	0.07	0.33	0.04	0.92	−0.30	1.00		
Mn	20.49	5.24	31.35	6.20	−0.39	1.00			
Fe	6.21	2.95	15.07	4.09	1.00				

Table 3-5-2 Morphology and Chemical Properties of Manganese Nodules

Morphology	(n)	Ni (%)				Cu (%)				Co (%)			
		Average	Standard deviation	Maximum	Minimum	Average	Standard deviation	Maximum	Minimum	Average	Standard deviation	Maximum	Minimum
Spheroidal	23	1.10	0.27	1.36	0.33	0.77	0.24	1.16	0.21	0.16	0.06	0.28	0.04
Ellipsoidal	11	1.04	0.09	1.18	0.94	0.96	0.10	1.09	0.75	0.09	0.03	0.12	0.05
Ellipsoidal fat	3	0.79	0.34	0.99	0.40	0.77	0.47	1.06	0.22	0.13	0.12	0.27	0.05
Pebble thin	28	0.95	0.26	1.27	0.44	0.69	0.25	0.99	0.25	0.17	0.06	0.30	0.10
Pebble	92	0.85	0.24	1.40	0.42	0.55	0.22	1.12	0.24	0.20	0.07	0.32	0.05
Massive	36	0.58	0.14	0.86	0.33	0.34	0.10	0.65	0.18	0.25	0.06	0.33	0.08
Plate	4	0.51	0.03	0.54	0.48	0.29	0.05	0.37	0.25	0.23	0.08	0.28	0.11
Others	8	0.61	0.12	0.74	0.42	0.35	0.09	0.51	0.23	0.22	0.08	0.30	0.10

Morphology	(n)	Mn (%)				Fe (%)				Cu/Ni*	Mn/Fe*
		Average	Standard deviation	Maximum	Minimum	Average	Standard deviation	Maximum	Minimum		
Spheroidal	23	23.51	4.12	30.80	13.40	7.29	2.63	14.59	4.14	0.70	3.61
Ellipsoidal	11	28.94	2.81	31.23	21.77	5.64	0.59	6.76	4.94	0.93	5.22
Ellipsoidal fat	3	26.35	7.89	31.35	17.26	8.06	4.76	13.55	5.16	0.89	4.31
Pebble thin	28	22.91	4.81	29.44	10.96	8.72	3.09	14.70	5.52	0.71	3.03
Pebble	92	19.52	4.53	30.16	10.54	9.39	2.72	15.06	4.09	0.63	2.32
Massive	36	17.82	3.13	23.24	9.56	11.05	2.41	15.07	4.97	0.58	1.66
Plate	4	14.38	5.10	18.47	7.73	11.52	1.29	12.73	9.71	0.58	1.25
Others	8	15.69	4.86	20.42	6.20	10.16	2.59	13.42	5.38	0.57	1.57

* Arithmetic average

㉯ Grade and Size

Table 3-5-3 shows grade characteristics classified by the size of manganese nodules. The results show that the small size manganese nodules have higher grades of Ni and Cu, and lower grades of Co and Fe.

The manganese nodules in the 8~16cm size group have lower grades of Ni, Cu, Mn and higher grades of Co, Fe than the other size groups. The conceivable cause might be the effect of rock fragments that constitute the core.

Table 3-5-3 Size and Chemical Properties of Manganese Nodules

Size (cm)	(n)	Ni (%)				Cu (%)				Co (%)			
		Average	Standard deviation	Max-imum	Min-imum	Average	Standard deviation	Max-imum	Min-imum	Average	Standard deviation	Max-imum	Min-imum
0 ~ 2	66	0.95	0.28	1.40	0.42	0.63	0.24	1.12	0.24	0.19	0.07	0.30	0.05
2 ~ 4	67	0.88	0.25	1.27	0.42	0.59	0.25	1.16	0.23	0.19	0.07	0.32	0.04
4 ~ 6	46	0.73	0.24	1.16	0.35	0.50	0.26	1.06	0.22	0.20	0.08	0.31	0.05
6 ~ 8	15	0.69	0.24	1.03	0.33	0.52	0.31	1.03	0.20	0.20	0.10	0.33	0.06
8 ~ 16	11	0.57	0.18	0.97	0.37	0.38	0.26	1.09	0.18	0.24	0.09	0.31	0.05

Size (cm)	(n)	Mn (%)				Fe (%)				Cu/Ni*	Mn/Fe*
		Average	Standard deviation	Max-imum	Min-imum	Average	Standard deviation	Max-imum	Min-imum		
0 ~ 2	66	20.47	4.61	28.78	10.88	8.70	2.74	15.06	4.60	0.65	2.67
2 ~ 4	67	20.96	5.42	30.80	6.20	8.95	2.88	14.43	4.09	0.65	2.70
4 ~ 6	46	19.94	5.52	31.35	7.73	9.90	3.09	14.70	5.16	0.66	2.35
6 ~ 8	15	21.31	6.36	31.23	9.56	9.62	3.61	15.07	4.97	0.71	2.72
8 ~ 16	11	18.87	5.21	30.86	11.46	10.38	2.66	13.55	4.95	0.62	2.06

* Arithmetic average

④ Grade and Topography

Table 3-5-4 shows grade characteristics classified by the topography. They can be summarized as follows:

(a) Plains, Channels and Sea knolls indicate similar grade tendencies containing high grade Ni, Cu and low grade Co, Fe.

(b) Platforms indicate the reverse of (a), i.e., low grade Ni, Cu and high grade Co, Fe.

Table 3-5-4 Sea Floor Topography and Chemical Properties of Manganese Nodules

Topography	(n)	Ni (%)				Cu (%)				Co (%)			
		Average	Standard deviation	Maximum	Minimum	Average	Standard deviation	Maximum	Minimum	Average	Standard deviation	Maximum	Minimum
Flat	48	0.76	0.24	1.34	0.49	0.49	0.23	1.08	0.29	0.22	0.07	0.31	0.05
Channel	1	0.68	—	—	—	0.53	—	—	—	0.12	—	—	—
Platform	1	0.42	—	—	—	0.22	—	—	—	0.30	—	—	—
Sea knoll	21	0.65	0.20	1.19	0.40	0.42	0.21	1.16	0.25	0.23	0.07	0.30	0.04

Topography	(n)	Mn (%)				Fe (%)			
		Average	Standard deviation	Maximum	Minimum	Average	Standard deviation	Maximum	Minimum
Flat	48	20.14	4.20	31.07	12.40	10.07	2.80	14.42	4.09
Channel	1	11.80	—	—	—	10.30	—	—	—
Platform	1	15.61	—	—	—	12.82	—	—	—
Sea knoll	21	19.25	3.77	30.81	8.07	11.44	3.00	14.49	4.14

⑥ Grade and Bottom Sediments

Grade characteristics classified by bottom sediments are shown in Table 3-5-5.

Manganese nodules distributed in the Siliceous clay have high grade Ni, Cu and low grade Co, Fe. On the contrary, in the Foraminifera ooze, the Ni, Cu grade is low and the Co, Fe grade is high. Brown clay and Calc-siliceous clay, show a medium grade of the aforesaid sediments. However, the manganese nodules in Brown clay indicate similar grade characteristics to Siliceous clay while those in Calc-siliceous clay are similar to the Foraminifera ooze.

Table 3-5-5 Bottom Materials and Chemical Properties of Manganese Nodules

Sediments	(n)	Ni (%)				Cu (%)				Co (%)			
		Average	Standard deviation	Maximum	Minimum	Average	Standard deviation	Maximum	Minimum	Average	Standard deviation	Maximum	Minimum
Brown clay	51	0.78	0.25	1.34	0.42	0.53	0.26	1.16	0.22	0.21	0.08	0.31	0.04
Siliceous clay	1	0.96	—	—	—	0.56	—	—	—	0.20	—	—	—
Calc-siliceous caly	17	0.65	0.15	1.30	0.52	0.37	0.09	0.84	0.28	0.25	0.04	0.29	0.12
Foraminifera ooze	2	0.41	0.02	0.44	0.40	0.25	0.00	0.25	0.25	0.29	0.01	0.30	0.28

Sediments	(n)	Mn (%)				Fe (%)			
		Average	Standard deviation	Maximum	Minimum	Average	Standard deviation	Maximum	Minimum
Brown clay	51	20.42	4.95	31.07	10.68	9.50	2.81	13.91	4.09
Siliceous clay	1	18.54	—	—	—	8.30	—	—	—
Calc-siliceous caly	17	18.36	1.91	23.79	8.07	11.97	2.13	14.42	6.44
Foraminifera ooze	2	19.11	0.14	19.33	19.03	14.36	0.08	14.49	14.31

⑥ Grade and CCD

In order to study the relation between the CCD and three principal components (Ni, Cu, Co), a triangular diagram is shown in Figure 3-5-15.
The CCD in this survey area is estimated at a water depth of about 5,000m as aforementioned, the grade characteristics of manganese nodules can be divided by the CCD into the following two groups according to this triangular diagram.

a. Ni, Cu rich type
b. Co rich type

Figure 3-5-16 shows the same relationship of the sampling points from where the abundance is over 5 kg/m^2. This figure indicates that all of the Ni, Cu rich type manganese nodules of over 5 kg/m^2 abundance are collected from depths of below 5,000m.

The relation between depth and the three principal components (Ni+Cu+Co) is shown in Figure 3-5-17. This figure is plotted by dividing the survey area into two zones; western part and eastern part of the Line Islands. The result shows that high grade manganese nodules are distributed in the range of water depth of 5,000~5,100m. In other words, high grade manganese nodules are distributed at or right under the CCD. Furthermore, at the western side of the Line Islands, high grade manganese nodules are distributed right under the CCD, and at the eastern side, they are distributed in the neighborhood of the CCD.

⑦ Mn/Fe Ratio and Manganese Nodules

It is a well-known fact that the ratio of Mn/Fe differs greatly according to the structural formation of manganese nodules (Bonatti et al., 1972).

The relation between Mn/Fe Ratio and (Ni+Cu+Co) grade is shown in Figure 3-5-18.

From this Figure 3-5-18, the manganese nodules can be classified into two types, divided at the Mn/Fe Ratio of 2.5. Based on this classification, a triangular diagram of Ni-Cu-Co is plotted as shown in Figure 3-5-19.
The relation between Mn/Fe Ratio and abundance is shown in Figure 3-5-20. Abundance, grade and depth are summarized in the Table 3-5-6.

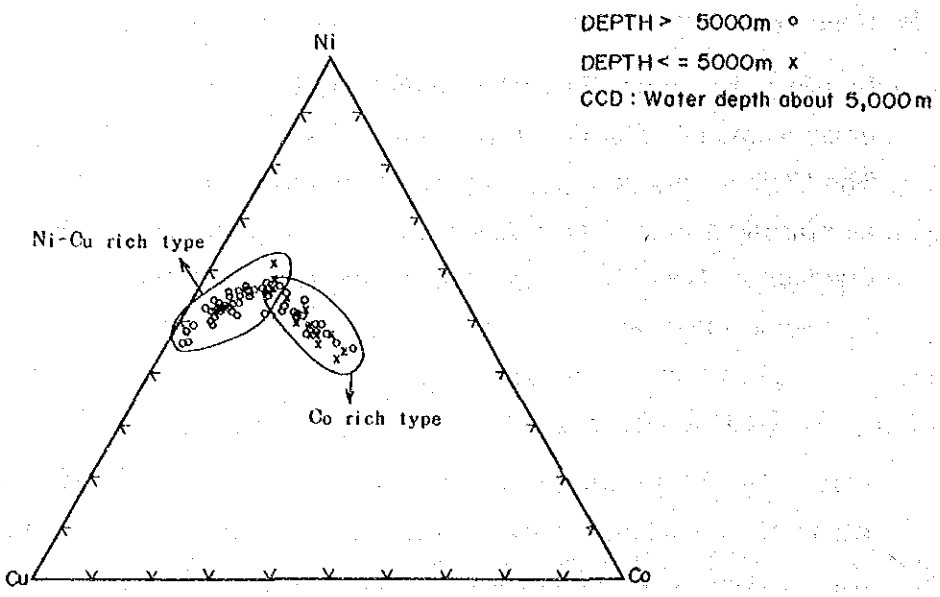

Figure 3-5-15 Triangular Diagram of Ni-Cu-Co by CCD (1)

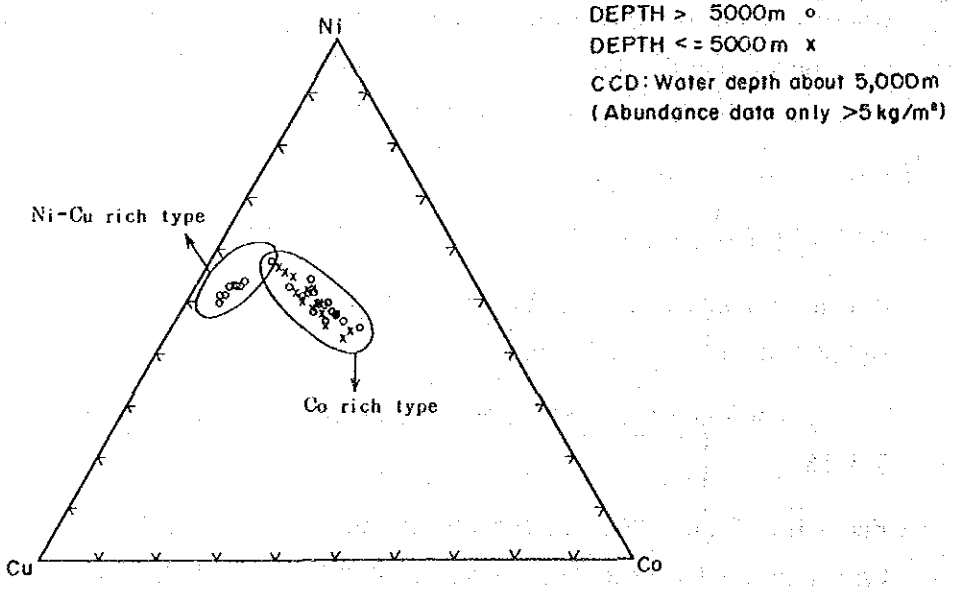

Figure 3-5-16 Triangular Diagram of Ni-Cu-Co by CCD (2)

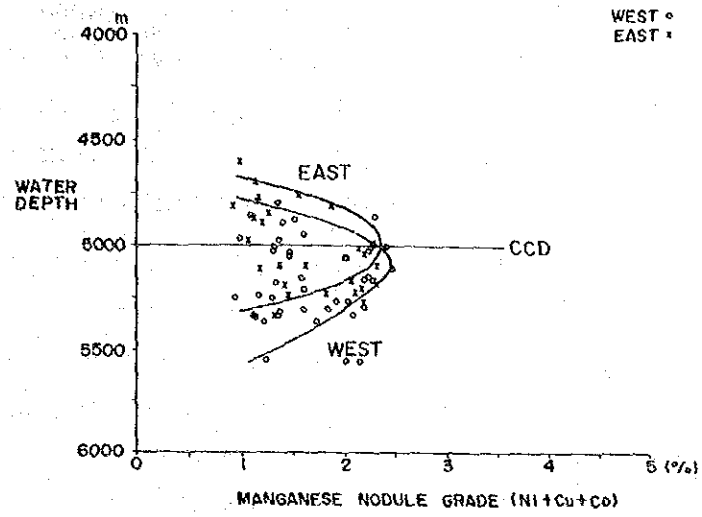

Figure 3-5-17 Relation of Water Depth and (Ni+Cu+Co) Grade

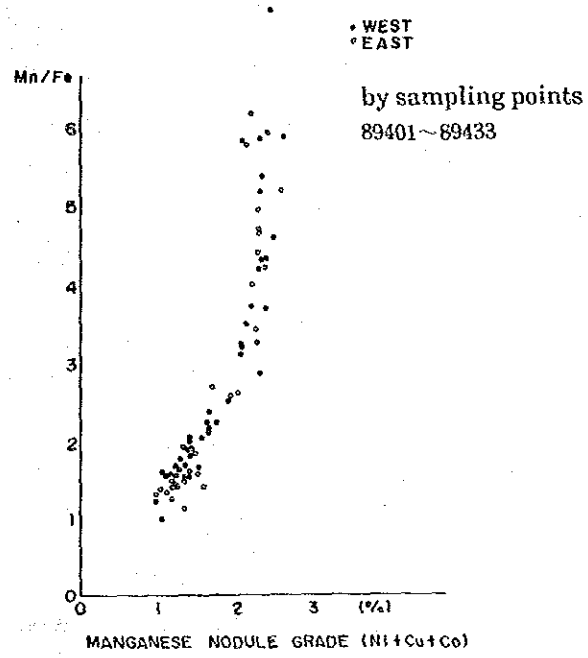

Figure 3-5-18 Relation of Mn/Fe and (Ni+Cu+Co) Grade

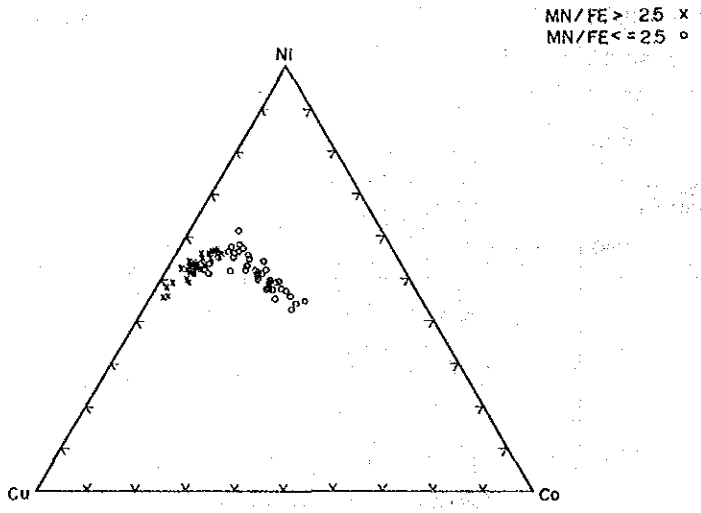

Figure 3-5-19 Triangular Diagram of Ni-Cu-Co by Mn/Fe

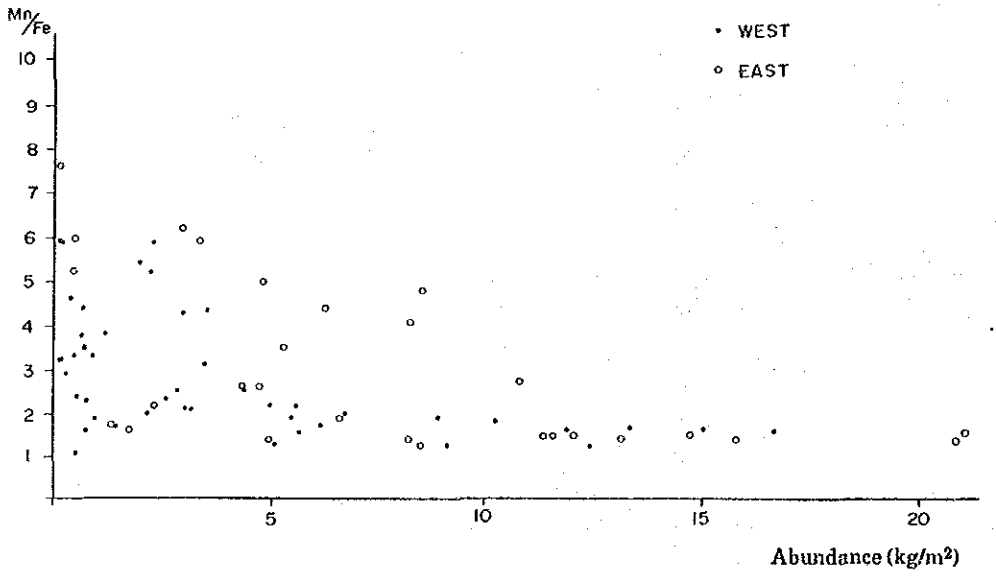

Figure 3-5-20 Relation of Mn/Fe and Abundance

The manganese nodules with more than 2.5 Mn/Fe Ratio correspond to the Ni, Cu rich type with low abundance. They are distributed in comparatively deep regions. On the contrary, the manganese nodules with Mn/Fe Ratio of below 2.5 correspond to the Co rich type with high abundance and distributed in the shallow regions.

Distribution map of Mn/Fe is shown in Figure 3-5-21. According to this map, most of the survey area is occupied by manganese nodules with Mn/Fe: 2 and up, but there are Mn/Fe: 1-2 zones in narrow area at the eastern and the western part of the Line Islands. Those zones are considered to correspond to the medium and high abundance zones described in the Abundance of Manganese Nodules (3-5, 2).
Among them, samples with Mn/Fe: 1-2, collected at the eastern sea area of the Line Islands, show particularly high average value of 12.02 kg/m^2 (average value of 4 sampling stations, 10 sampling points). This figure is about three times higher than the average abundance (4.37 kg/m^2) of the whole survey area.

Figure 3-5-22 shows the Distribution map of manganese nodules Mn/Fe in the Pacific Ocean. According to this map the survey area shows a tendency toward high Mn/Fe ratio. It is assumed that zones of manganese nodules with Mn/Fe: 2-5 distributed to the east of this survey area are also distributed in this area. The characteristics and distribution of the manganese nodules with Mn/Fe: 1-2 are worthwhile to study in the future.

Table 3-5-6 Characteristics classified by Mn/Fe

	Mn/Fe > 2.5	Mn/Fe < 2.5
Abundance	Low (Av. 2.7 kg/m^2)	High (Av. 7.5 kg/m^2)
Grade	Ni, Cu → High (1.08%) (0.78%) Co → Low (0.13%)	Ni, Cu → Low (0.61%) (0.35%) Co → High (0.26%)
Water Depth	5,000~5,500m min. 4,810m~max. 5,560m * most of them are in the deep sea of 5,000~5,200m	4,700~5,300m min. 4,600m~max. 5,550m * those with abundance of 10 kg/m or over are located in the depth of 4,700~5,000m

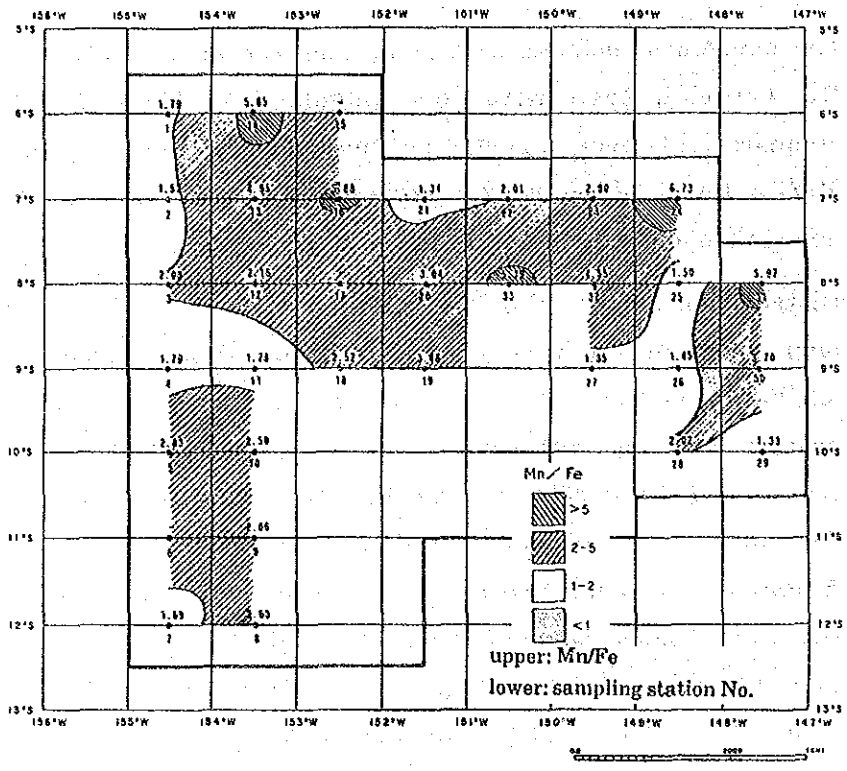

Figure 3-5-21 Distribution Map of Manganese Nodules Mn/Fe

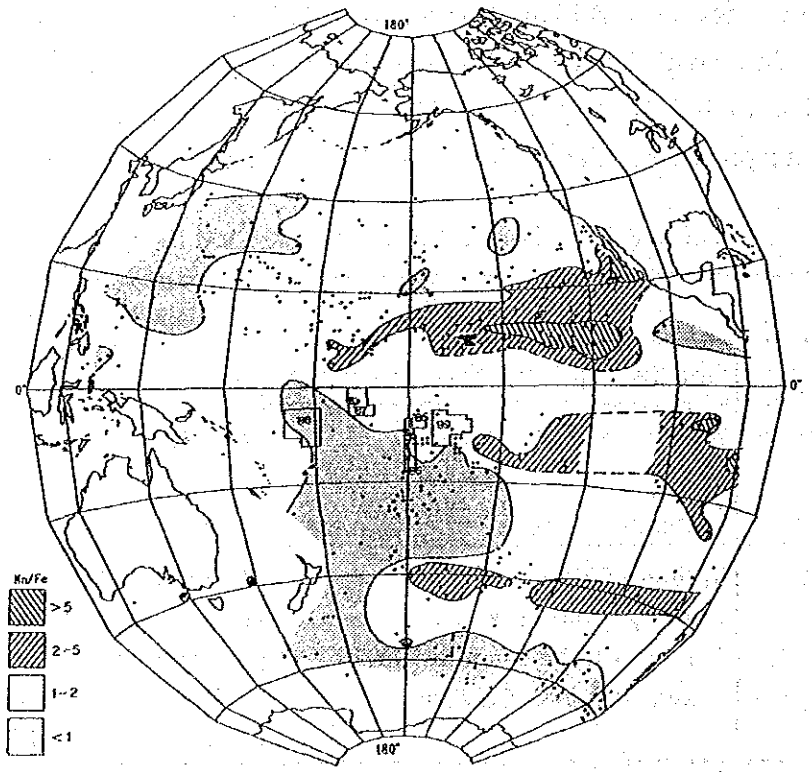

Distribution of Mn/Fe ratios in ferromanganese nodules from the Pacific (from Calvert, 1978).
Underwater Minerals
By D.S.CRONAN

Figure 3-5-22 Distribution Map of Manganese Nodules Mn/Fe in the Pacific Ocean

(3) Auxiliary components

In order to determine characteristics of the auxiliary components of manganese nodules, major and minor elements analysis were carried out on six representative samples selected from among the samples that had undergone on-board analysis for five principal components. The results of the major and minor elements analysis, together with the results of on-board-analysis, are shown in Table 3-5-7. Characteristics can be summarised as follows;

From analysis of values of Ni, Cu, Co of the six samples, two samples (89S1147FG03 and 89S1341FG02) can be classified as Co rich types and the remaining four samples as Ni, Cu rich types.

① SiO_2 content ranges from 11.48% to 21.32%. The average of six samples is about 16%.

② In case of Fe_2O_3 > FeO, shows rich in ferric iron.
Among the six samples, Co rich type manganese nodules have more content of Fe_2O_3 than the other type.

③ The following differences between the Co rich types and the Ni, Cu rich types were determined by microanalysis.

Co rich types were rich in components: Pb, Sr, V, As, Zr, ΣR_2O_3*1

Ni, Cu rich types were rich in components: Zn, Mo

④ The following difference were found between the results of these analyses and the average grade*2 of manganese nodules in the Clarion-Clipperton Prime Area reported by Mackelvey et al., (1979):

High content components in this survey area:
SiO_2, Al_2O_3, CaO, Na_2O, K_2O, P_2O_5, V

High content components in the Clarion-Clipperton Prime Area:
Zn, Sr, Mo, B

---

*1 ΣR_2O_3 shows contents of total rare earth elements.

*2 Si 7.81%, Ti 0.61%, Al 2.84%, Mg 1.80%, Ca 1.47%, Ba 0.32%, Na 1.87%, K 0.82%, P 0.23%, Pb 0.048%, Sr 0.066%, Mo 0.048%, V 0.03%, B 0.016%, Zn 0.13%, Y 0.01%

Table 3-5-7 Analyses of Major and Minor Elements of Manganese Nodules

Sample No.		89S0942 FG03	89S0845 FG02	89S0948 FG03	89S1147 FG03	89S1341 FG02	89S1141 FG02
Topography		(Hilly) Flat	(Quasi) Seaknoll	(Quasi) Flat	(Quasi) Flat	(Plain) Flat	(Plain) Flat
Depth (m)		5,060	5,100	5,230	4,790	5,370	5,560
Morphology		Pebble	Pebble thin	Ellipsoidal	Ellipsoidal fat	Massive	Spheroidal
Size (cm)		2-4	4-6	8-16	8-16	8-16	0-2
Major Metal Contents (%)	Ni	1.02	0.94	0.97	0.40	0.40	1.15
	Cu	0.68	0.66	1.09	0.22	0.20	0.72
	Co	0.12	0.11	0.05	0.27	0.31	0.19
	Mn	16.49	17.70	30.86	17.26	18.00	23.78
	Fe	5.79	6.63	4.95	13.55	12.10	7.53
Major Element Contents (%)	SiO_2	18.60	15.26	11.48	21.32	15.26	14.00
	TiO_2	1.08	0.46	0.32	0.87	1.27	0.80
	Al_2O_3	6.24	5.85	4.13	6.58	5.64	6.63
	Fe_2O_3	15.51	9.33	7.93	18.80	17.76	10.87
	FeO	0.19	0.19	0.32	0.06	0.19	0.32
	MnO_2	27.41	39.25	46.10	23.06	29.59	36.44
	MgO	2.71	3.11	3.71	2.06	1.18	3.78
	CaO	1.88	2.06	2.03	2.32	2.40	1.85
	BaO	0.39	0.47	0.57	0.31	0.33	0.29
	Na_2O	2.64	2.33	2.47	2.47	2.45	2.54
	K_2O	1.70	1.54	1.12	1.30	1.02	1.32
	P_2O_5	0.60	0.54	0.41	0.66	0.60	0.51
	Ig-loss	21.34	20.43	21.00	19.96	23.03	21.26
Minor Element Contents (ppm)	Pb	589	216	180	541	865	481
	Zn	714	1,189	1,326	497	472	918
	Sr	272	190	228	281	315	190
	V	332	275	216	323	385	307
	Mo	318	359	441	283	336	400
	B	220	157	125	243	233	172
	As	120	64	45	128	147	84
	Y	97	97	78	115	99	90
	Zr	439	236	172	428	418	314
	Pt	0.6	0.3	0.2	0.3	0.2	0.2
	ΣR_2O_3	936	509	372	1,044	975	622

4) Mineral Composition

Powder X-ray diffraction and microscopic observation were carried out on representative samples to investigate the mineral composition and internal structure of the manganese nodules. Representative samples were selected from the manganese nodules classified as Ni-Cu rich types and Co rich types according to the values of analysis. X-ray diffraction and microscopic observation were carried out on representative samples of each type.

	Ni-Cu rich Type	Co rich Type
Sample No.	89S0842SC01	89S0947FG01
Water Depth	5,170m	5,110m
Morphology	Ellipsoidal type	Massive type
Size	25×18mm	50×47mm
Grade:		
Ni (%)	1.18	0.56
Cu (%)	0.95	0.35
Co (%)	0.12	0.28
Mn/Fe	5.39	1.48

(1) X-ray Diffraction

As the size of the Ni-Cu rich type test pieces was small, all of them were treated as a bulk sample for powder diffraction. Powder X-ray diffraction on the Co rich type samples was carried out by classifying the samples into outer shell, mid-shell, inner shell and upper layer, lower layer.

The results of X-ray diffraction are shown in Table 3-5-8. A typical X-ray chart is shown in Figure 3-5-23; the result shows that the Ni-Cu type is composed of 10Å manganite and δ-MnO_2 while the Co type is prominent in δ-MnO_2 with 10Å manganite appearing only in the lower layer and outer shell. These facts conform to the theory of Usui (1983) which states that the 10Å manganite is rich in Cu, Ni, Zn, while δ-MnO_2 is rich in Co, Pb and only the lower layer and the outer shell, which directly come in contact with bottom materials, are composed of 10Å manganite and the upper layer, which reacts directly with sea water, is predominately δ-MnO_2. A small amount of phillipsite and quartz are contained as gangue minerals.

Table 3-5-8 Results of X-ray Diffraction Analysis of Manganese Nodules

Sample No.	Size (cm)	Morphology	Portion		10 Å	δ-Mn	Ph	Q
89S0947FG01	4 ~ 6	Massive	Upper	outer		⫲	+	±
				middle		⫲	±	⫲
				inner		⫲	±	+
			Lower	inner		⫲	±	+
				middle		⫲	±	+
				outer	+			
89S0842SC01	2 ~ 4	Ellipsoidal	Bulk		⫲	⫲	+	

Legend 10 Å : Manganite δ-Mn : δ-MnO_2 Ph : Phillipsite Q : Quartz
⫲ : Reflection is very strong ⫲ : Refleciton is strong
+ : Reflection is weak ± : Reflection is very weak or obscure
Cu-Monochrometer 45kV, 20 mA

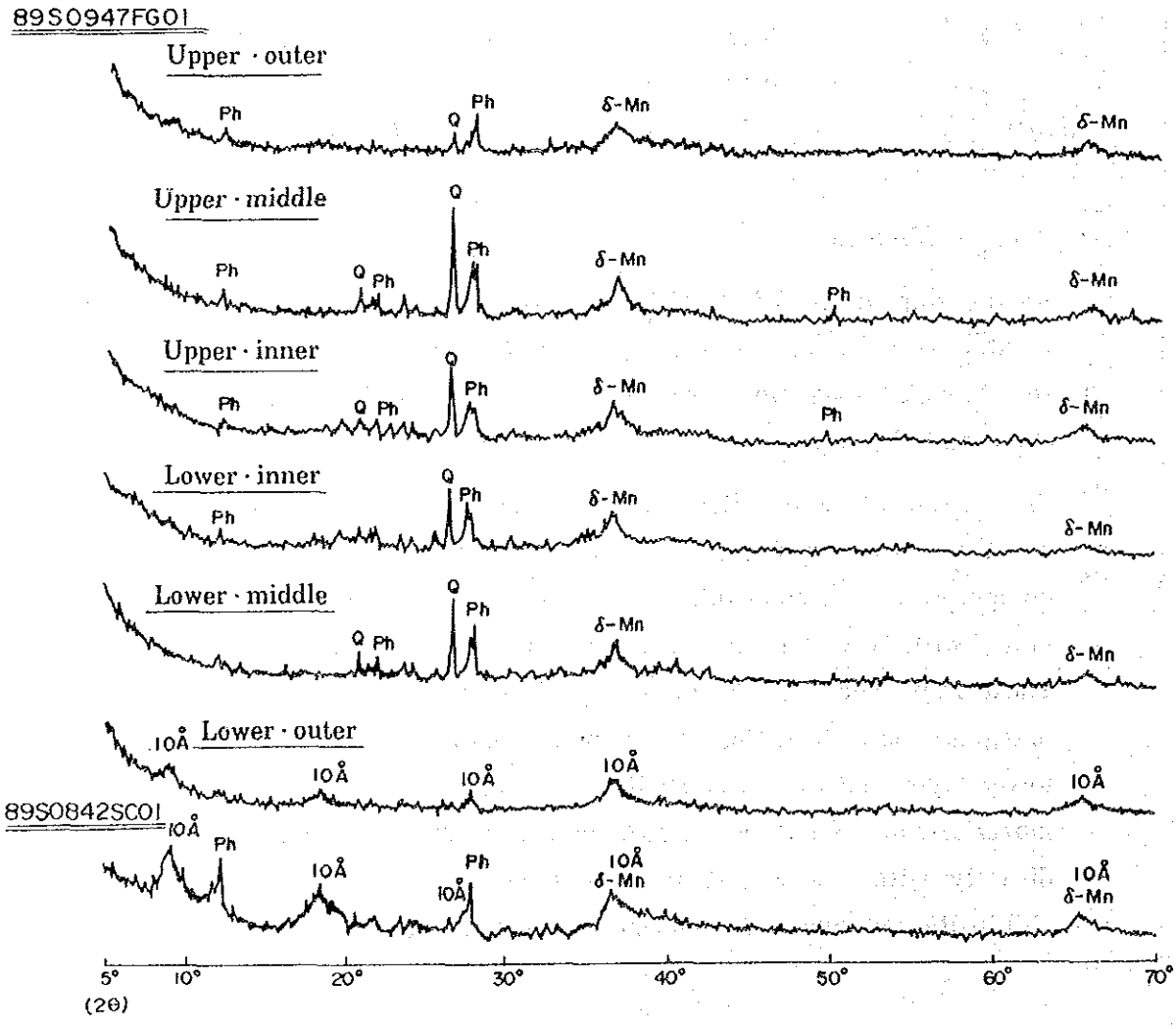

Legend 10Å : Manganite δ-Mn : δ-MnO_2 Ph : Phillipsite Q : Quartz

Figure 3-5-23 X-ray Diffraction Patterns of Manganese Nodules

(2) Microscopic Observation

① 89S0842SC01 (Ni-Cu rich Type)

The core is composed of sliceous material and the outer side is stratified textures of hematite, goethite and 10Å manganite. δ-MnO_2 is not recognized. Further to the outermost, δ-MnO_2, 10Å manganite, stratified textures and dendric textures of goethite are observed. Some of the goethite are in the forms of botryoidal, pool and irregular granulose. The outermost layer is rich in colloform structure composed of 10Å manganite, δ-MnO_2 and goethite. δ-MnO_2 is colored gray to light gray with a green tint. As a whole, outer layer is rich in δ-MnO_2. 10Å manganite and inner layer rich in goethite and hematite.

② 89S0947SC01 (Co rich Type)

The core is composed of quartz, altered plagioclase, calcite, montmorillonite. At the inner shell, microscopic stratified texture (width under 0.05-0.1mm), reniform texture, dendritic texture of δ-MnO_2, 10Å manganite and goethite are observed. Calcite and lutaceous materials are imbedded in the interstices of the minerals. In the mid shell there are reniform and dendritic stratified texture composed of δ-MnO_2, 10Å manganite and goethite. The outer shell is predominately microscopic colloform (width of about 0.01mm) composed of δ-MnO_2, 10Å manganite and goethite. 10Å manganite is recognized in every layer, though it rarely appeared at the X-ray diffraction.

5) Results of CDC Survey

With the object of estimating the abundance of manganese nodules and grasping its continuity, CDC survey was implemented at a trackline (about 5.4 miles long) in the high abundance zone located at the eastern part of the survey sea area. The said survey was implemented in the direction from 148°30'W to 148°24'W along 9°00'S (sampling station 89426), and 188 photographs were taken at approx. 50m intervals.

Location map of CDC trackline is shown in Figure 3-5-24. Statistics of CDC measurements are shown in Table 3-5-9. Variation charts of topography, abundance and coverage determined from the photographs are shown in Figure 3-5-25. Examples of CDC continuous photographs are shown in Fig. 3-5-26. Typical CDC photographs are shown in Figure 3-5-27.

(1) Abundance

The results show that the survey area is poor in continuity of abundance and that alterations of abrupt variation of abundance are too often recognized. This specific character is consistent with the sampling results.

Cyclic variation of abundance is recognized from the western part of the sea area to the central part of 148°28.5'W (Photo No. 100) with the cycle of about 2,500m, but this cycle fluctuates to 1,500m and then to 1,000m at the eastern part of the area. Abundance decreases at the eastern part of the area (abundance at the starting point of the survey is about 15 kg/m^2 and about 5 kg/m^2 at the final point).

There are stations of low abundance at the central part of the trackline (148°28'W, Photo Nos. 112-136) and to the eastern part of 148°26'W (Photo Nos. 165-188). The topography of these sections indicates rocky knolls with prominent plate-type manganese nodules and manganese crusts.*1

Small pebble type manganese nodules (about 2cm in diameter) are prominent in the neighborhood of the trackline, so the value of abundance is low (average of 8.13 kg/m^2) though there is a high coverage (average of 37.4%).

The relation between abundance and water depth is not obvious but the abundance in knoll zones is low and at the water depth of less than 4,900m, decrease of abundance is also recognized.

---

*1 Manganese crusts were excluded from coverage, abundance calculation.

(2) Morphology

The morphology of manganese nodules judged from the CDC photographs indicates the prominence of pebble type nodules, but there are also various types of nodules such as massive, plate and spheroidal. Pebble type manganese nodules with diameter of about 2cm are distributed widely in the vicinity of the track line. Massive types are also distributed throughout the trackline. Plate type manganese nodules and manganese crusts are recognized at the central part and the eastern part of the trackline.

Table 3-5-9 Statistics of CDC Measurements

	Coverage *2 (%)	Abundance *3 (kg/m^2)
Samples collected *1	162	162
Maximum value	94.0	21.99
Minimum value	0.0	0.00
Mean value	37.4	8.13
Standard deviation	23.8	5.73

*1 Total number of photographs taken was 188, but 26 of them were excluded as irrelevant to the subject.

*2 Point counting method is applied to the measurement of area rate.

*3 Calculation of abundance was based on the following formula:

$C=0.245171\times Z - 1.05799$

C: Abundance Z: Coverage

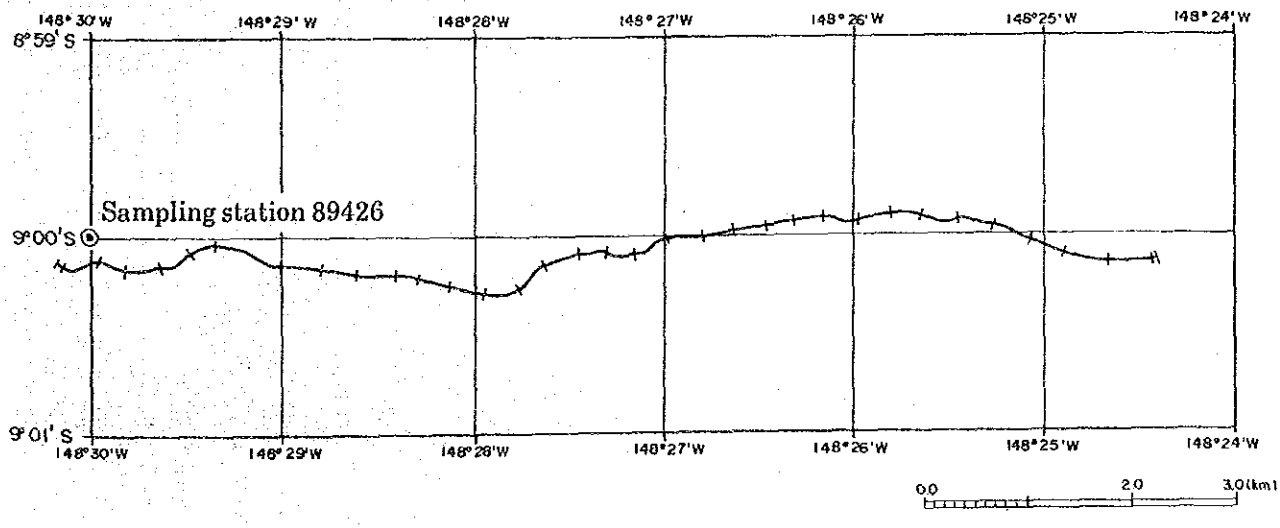

Figure 3-5-24 Location Map of CDC Trackline(Trackline 89SCDC01)

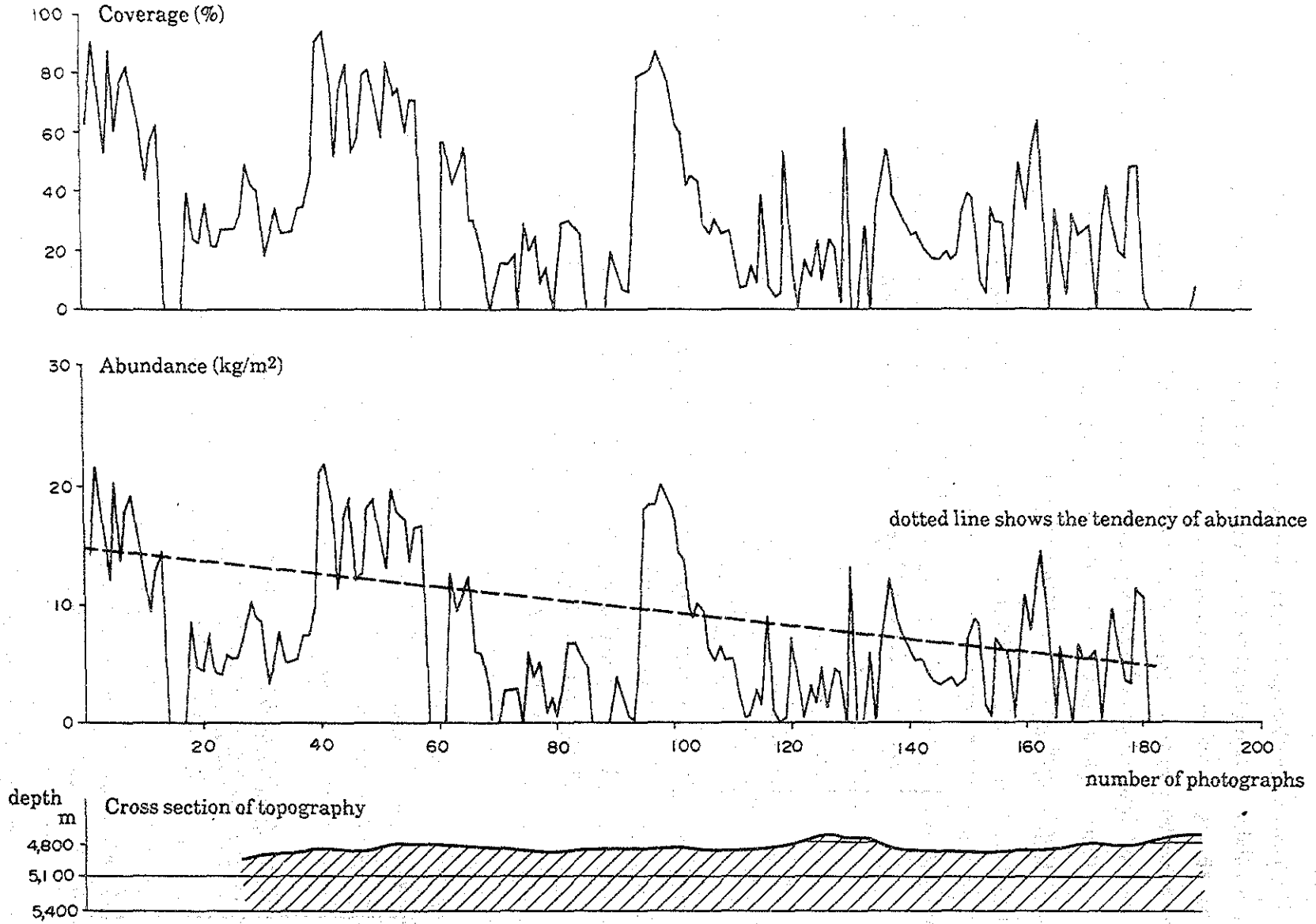

Figure 3-5-25 Variation Charts of Topography, Abundance and Coverage (Trackline 89SCDC01)

006～010

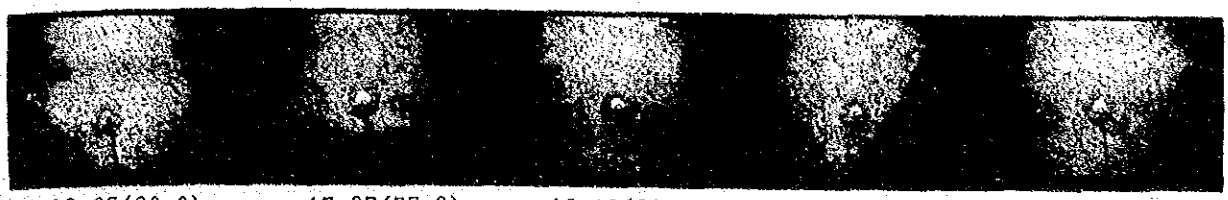

13.65(60.0) 17.87(77.2) 19.12(82.3) 15.96(69.4) 13.75(60.4)

Continuous distribution of Pebble type Manganese Nodules

154～158

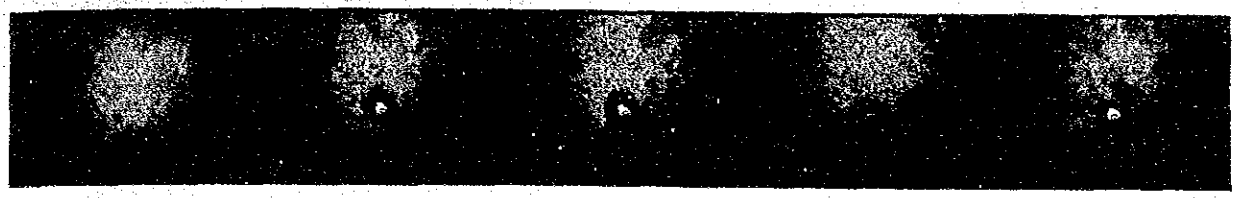

0.39(5.9) 7.50(34.9) 6.15(29.4) 6.13(29.3) 0.27(5.4)

Distribution of Pebble type and Massive type Manganese Nodules. Low abundance.

096～100

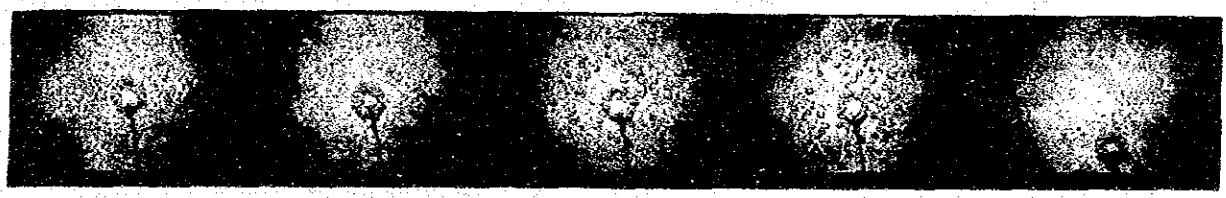

18.53(79.9) 18.58(80.1) 20.30(87.1) 19.17(82.5) 18.16(78.4)

Distribution of Pebble type as well as Spheroidal type Manganese Nodules. Diameter: about 5cm.

084～088

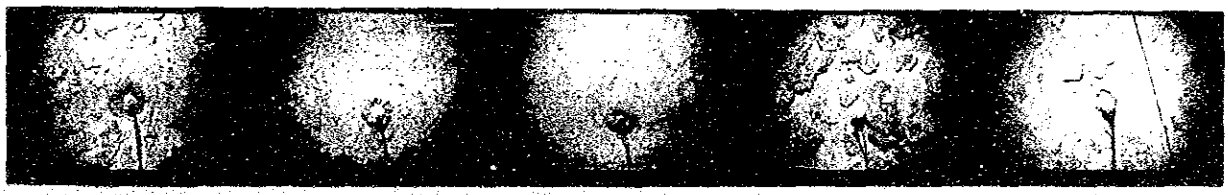

5.76(27.8) 5.00(24.7) 0.00(0.5) 7.52(35.0) 6.30(30.0)

Distribution of Plate type Manganese Nodules

125～129

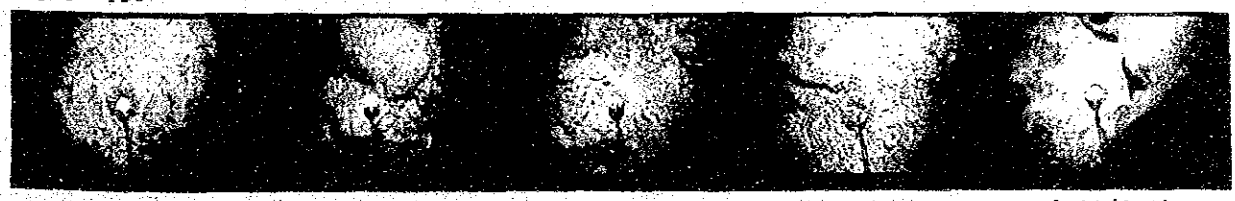

4.56(22.9) 0.00(0.0) 4.58(23.0) 4.24(21.6) 0.00(0.0)

Exposed Bedrock Zone. Occurrence of thin Manganese Crust.
[Number at left-above: photo number, left below: abundance (kg/m^2), right below: coverage (%)]

Figure 3-5-26 Examples of CDC Continuous Photographs

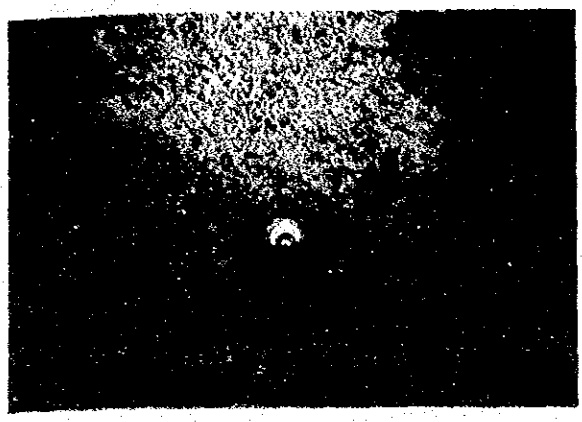

Pebble type: Abundance 19.12 kg/m^2

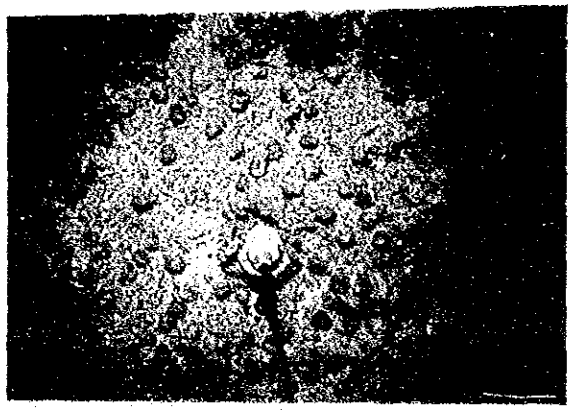

Spheroidal type and Pebble type:
Abundance 19.17 kg/m^2

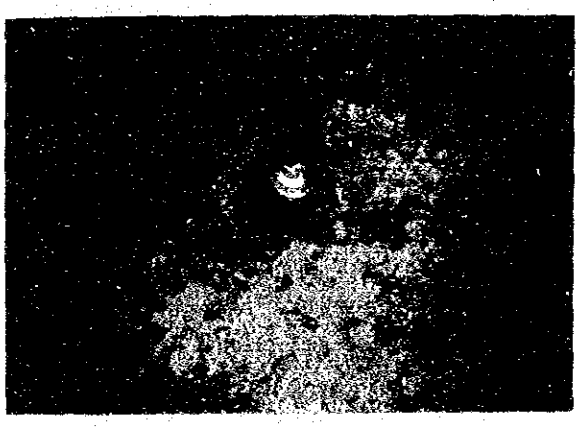

Massive type: Abundance 2.89 kg/m^2

Clay and Sea Bottom Organism:
Abundance 0.00 kg/m^2

Plate, Massive and Pebble types:
Abundance 16.47 kg/m^2

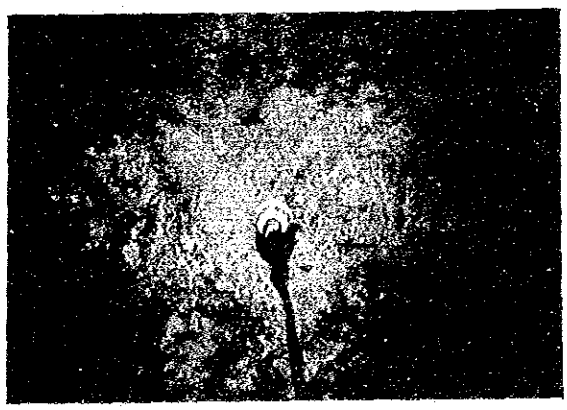

Manganese Crust: Abundance 0.00 kg/m^2
(Numbers are photograph numbers)

Figure 3-5-27 CDC Photographs

6) Metal Content

In assessing the resource potential of manganese nodules, it is necessary to consider not only the amount of manganese nodules in a unit area but also the metal content (particularly the target metals such as Ni, Cu, Co) of the manganese nodules.

Metal density (amount of metal in a unit area) of Ni, Cu, Co was calculated as follows for each sampling station. The results are shown in Figure.

Ni density = abundance × (1-water content) × Ni grade
Cu density = abundance × (1-water content) × Cu grade
Co density = abundance × (1-water content) × Co grade

Cut-off are not set for abundance and grade.

(1) Ni (Annexed Figure 16)

Total area with Ni content of 20 g/m^2 or above is 116,607 km^2 and its average density is 33.96 g/m^2.

(2) Cu (Annexed Figure 17)

Total area with Cu content of 20 g/m^2 or above is 55,426 km^2 and its average density is 28.2 g/m^2.

(3) Co (Annexed Figure 18)

Total area with Co content of 20 g/m^2 or above is 14,126 km^2 and its average density is 25.06 g/m^2.

As characteristics of metal content in the survey area, high metal densities of Ni, Cu, Co are recognized in the eastern sea area of the Line Islands, consistent with previously stated high abundance zones.

3-6 Discussions

1) As a result of analysis, manganese nodules were classified according to the Mn/Fe Ratio. The existence of two different types divided at about Mn/Fe = 2.5 was recognized. (Figure 3-6-1)

Ni-Cu rich Type (Mn/Fe > 2.5)

① Abundance is low (average 2.7 kg/m^2).

② Among Ni-Cu-Co, percentages of Ni grade and Cu grade are high.

	Grade	Percentage
Ni :	1.08%	(54%)
Cu :	0.78%	(39%)
Co :	0.13%	(7%)
Metal density		3.87 g/m^2

③ Occur on the sea bottom (water depth: 5,000 - 5,200m) slightly deeper than the CCD (water depth: 5,000m)

④ Occur in sea areas of Brown clay distribution.

⑤ Occur in the Plain zones.

⑥ Morphologically, abundant in ellipsoidal type, pebble thin type, spheroidal type, etc.

⑦ Manganese oxide is composed of 10Å manganite and δ-MnO_2.

⑧ Among trace components, rich in Zn.

Co rich Type (Mn/Fe ≦ 2.5)

① Abundance is high (average 7.5 kg/m^2).

② Among Ni-Cu-Co, percentage of Co grade is high.

	Grade	Percentage
Ni :	0.61%	(50%)
Cu :	0.35%	(29%)
Co :	0.26%	(21%)

Metal density 6.59g/m^2

③ Occur on the sea bottom (water depth: 4,700 - 5,000m) directly above and below the CCD (water depth: 5,000m)

④ Occur in sea area of calcareous sediments distribution.

⑤ Occur in the regions prominent in Seaknolls, etc.

⑥ Morphologically, abundant in pebble type massive type, plate type, etc.

⑦ Manganese oxide is predominantly δ-MnO_2.

⑧ Among trace components, rich in Pb, ΣR_2O_3, etc.

2) The survey sea area has a wide distribution of Ni-Cu rich type, in the aggregate, abundance is low. However, in the vicinity of 9°S, at the eastern and western sea areas of the Line Islands, distribution of Co rich type is observed. Local high abundance is recognized at these areas.

3) Even in the sea area with high abundance on the average, the zones where sea floor topography shows knolls or rocks, are prominent in small-sized pebble type manganese nodules. Consequently the abundance at such places is low.

4) Above mentioned phenomenon is also a tendency of previous surveys. Accordingly, in relation to the distribution of manganese nodules in the South Pacific Ocean, it is recommended that the survey be done at a newly selected sea area in the future with those principles.

Ni-Cu rich Type (Mn/Fe > 2.5)

① Low abundance (average: 2.7kg/m²)

③ Among Ni-Cu-Co, percentage of Ni grade and Cu grade are high.

	Grade	Percentage
Ni :	1.08%	(54%)
Cu :	0.78%	(39%)
Co :	0.13%	(7%)

Metal density : 3.87g/m²

③ Occur on the sea bottom (water depth: 5,000~5,200m) slightly deeper than the CCD (5,000m).

④ Occur in sea areas of Brown clay distribution.

⑤ Occur in Plain zones.

⑥ Abundant in ellipsoidal type, pebble thin type, spheroidal type.

Co rich Type (Mn/Fe ≤ 2.5)

① High abundance (average: 7.5kg/m²)

② Among Ni-Cu-Co, percentage of Co grade is high.

	Grade	Percentage
Ni :	0.61%	(50%)
Cu :	0.35%	(29%)
Co :	0.26%	(21%)

Metal density : 6.59 g/m²

② Occur on the sea bottom (water depth: 4,700~5,000m) directly above and below the CCD (5,000m).

④ Occur in sea areas of calcareous sediments.

⑤ Occur in the regions prominent in Seaknolls, etc.

⑥ Abundant in pebble type, massive type, plate type.

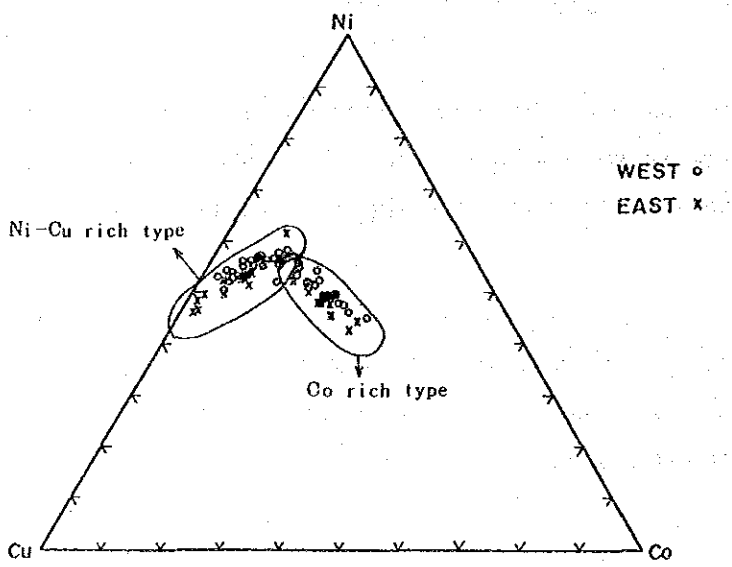

Figure 3-6-1 Ni-Cu-Co Triangular Diagram (Manganese Nodules)

Chapter 4. Results of Survey 2 (Cobalt Crusts)

4-1 Seamount Topography

Six seamounts were selected as subjects for the survey of cobalt crusts, all of them belonging to the Line Islands line. As previously stated in section 3-1, 1), the Line Islands line is composed of two series. The seamounts SC01-04 belong to the eastern seamount line and SC05-06 belong to the western seamount line.

Because of the lack of accurate age data, many theories had been proposed on the origin of the Line Islands line. Recently, Schlanger et al. (1984) published a reliable age data of the Line Islands by adopting ^{40}Ar-^{39}Ar Total Fusion Method. Figure 4-1-1 shows the data published by Schlanger et al. (1984). According to their data, the central part of the sea area shows the values of 71.9±1.4Ma and 70.5±1.1Ma and the age of origin is earlier as the distance from Line-Tuamotu Bend increases. Coral limestone dating from the Eocene, the Pliocene and the Pleistocene eras was acquired by dredging in Caroline Island area. (Schlanger et al. 1984).

Epp. (1984) proposed a formation model of the Line Islands line. The theory was based on the Schlanger age dating and the hypothesis that the Line Islands line was formed by the result of mutual interference of Pacific/Farallon Spredding Axis and Hot Spot between 130Ma to 67Ma.

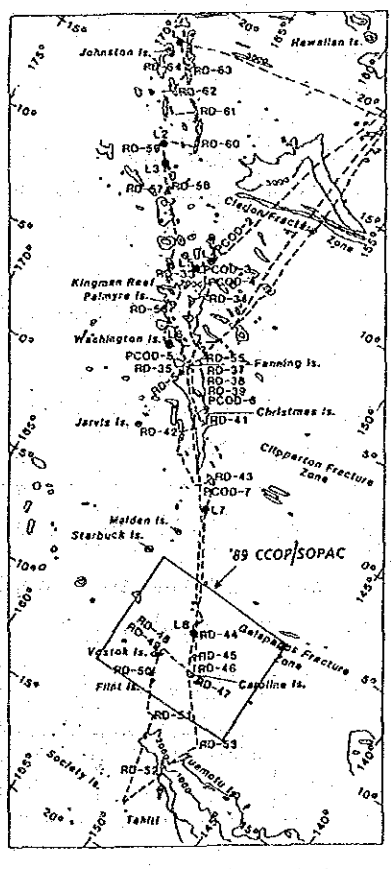

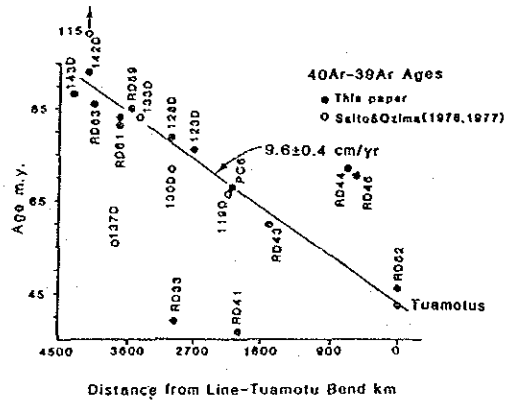

(Notes) By ^{40}Ar–^{39}Ar total fusion method, from Schlanger et al. (1984)

Figure 4-1-1 Established Age Dating of the Line Islands line

1) Classification

All of the seamounts selected as subjects of the survey belong to the Line Islands line are classified as peaked seamounts. However, SC01 seamount has ridges and SC05 seamount can be classified as a table reef. No typical guyot was found in this sea area, but SC01, SC02 and SC03 had small-scaled flats on their summits. Numerous coral fragments were collected from SC02 seamount. Accordingly, it is presumable that they were formed by the actions of coral-creation and wave-erosion and then preserved by the effects of sudden precipitation. In this sense, SC01, SCO02 and SC03 seamounts can be classified as guyots.

Classification of Seamount Topographic Types is shown in Table 4-1-1.

Table 4-1-1 Classification of Seamount Topographic Types

Classification	Morphological Characteristics
Peaked Seamount	The summit is steeple-shaped or ridge-shaped.
Guyot	The summit is flat and horizontal.

Seamount topography is defined as Table 4-1-2.

Table 4-1-2 Classification of Seamount Topography

Classification		Topographical Characteristics
The top	Central part	The center of the summit where it is flat or gently inclined.
	Shoulder	The transitional zone from the central part of the top to the upper part of the slope.
The slope	Upper part	The upper part where the slope is steep.
	Middle part	The lot between the upper and the lower part of the slope. The inclination is medium.
	Lower part	The lower part where the slope is gentle.

Table 4-1-3 shows the Area and Average slope of each seamount classified by above standards.

Table 4-1-3 Area and Average Slope of Each Seamount

	Depth Range (m)	Area (km^2)	Average slope	Minimum	Maximum	0-10°	10-20°	20-30°	30° <
SC01 Seamount (N)									
Flat summit	0 - 2,000m	61.60	7.1°	1.0°	17.4°	77.0%	23.0%	.0%	.0%
Upper slope	2,000 - 3,000m	340.76	10.8°	1.4°	20.1°	38.9%	60.5%	.6%	.0%
Middle slope	3,000 - 4,000m	604.90	9.2°	.4°	22.5°	54.8%	44.2%	1.0%	.0%
Lower slope	4,000 -	1052.08	5.2°	.0°	16.5°	83.2%	16.8%	.0%	.0%
SC01 Seamount (S)									
Flat summit	0 - 2,000m	96.58	9.2°	.5°	20.2°	61.1%	37.9%	1.1%	.0%
Upper slope	2,000 - 3,000m	300.51	12.7°	.7°	23.8°	30.1%	61.6%	8.2%	.0%
Middle slope	3,000 - 4,000m	647.96	10.3°	.5°	22.1°	48.7%	50.9%	.3%	.0%
Lower slope	4,000 -	1020.04	5.8°	.1°	18.8°	82.2%	17.8%	.0%	.0%
SC02 Seamount									
Flat summit	0 - 1,500m	25.14	8.5°	.4°	27.3°	64.6%	31.3%	4.0%	.0%
Upper slope	1,500 - 2,500m	232.54	13.8°	.7°	28.5°	28.8%	54.7%	16.5%	.0%
Middle slope	2,500 - 3,500m	755.66	12.3°	.1°	28.7°	33.4%	57.6%	9.0%	.0%
Lower slope	3,500 -	3123.99	5.6°	.0°	39.4°	84.6%	13.0%	2.2%	.3%
SC03 Seamount									
Flat summit	0 - 1,500m	18.37	9.8°	1.0°	23.2°	58.3%	38.9%	2.8%	.0%
Upper slope	1,500 - 2,500m	237.31	13.6°	.5°	26.4°	20.1%	69.5%	10.3%	.0%
Middle slope	2,500 - 3,500m	690.82	11.8°	.2°	27.9°	37.6%	55.1%	7.3%	.0%
Lower slope	3,500 -	1831.02	6.2°	.0°	31.1°	78.6%	20.4%	1.0%	.0%
SC04 Seamount									
Flat summit	0 - 1,700m	62.26	10.1°	.4°	25.0°	51.2%	43.4%	5.3%	.0%
Upper slope	1,700 - 2,500m	102.31	18.3°	2.0°	34.2°	10.1%	49.0%	38.9%	2.1%
Middle slope	2,500 - 3,500m	276.43	16.3°	.5°	35.7°	10.8%	65.9%	23.2%	.1%
Lower slope	3,500 -	1025.04	7.3°	.0°	32.9°	71.0%	26.0%	3.0%	.0%
SC05 Seamount									
Flat summit	0 - 500m	1.02	12.1°	12.1°	12.1°	.0%	.0%	.0%	.0%
Upper slope	500 - 2,000m	164.36	17.1°	1.4°	28.3°	16.7%	46.2%	37.2%	.0%
Middle slope	2,000 - 3,500m	575.07	12.9°	1.2°	23.9°	26.0%	67.6¥	65.5%	.0%
Lower slope	3,500 -	3530.69	4.4°	.0°	23.5°	89.8%	10.1%	.1%	.0%
SC06 Seamount									
Flat summit	0 - 1,500m	6.15	11.9°	3.1°	16.6°	16.7%	83.3%	.0%	.0%
Upper slope	1,500 - 2,500m	63.44	18.3°	5.0°	25.4°	6.7%	50.0%	43.3%	.0%
Middle slope	2,500 - 3,500m	137.65	17.4°	4.6°	24.5°	4.6%	67.2%	28.2%	.0%
Lower slope	3,500 -	2762.53	3.8°	.0°	23.8°	91.9%	8.0%	.1%	.0%

2) Topographic Features

The topographic features of individual seamounts are shown in Table 4-1-4. The topographic plans and sections of individual seamounts are shown in Annexed Figure 20. Bird's eye views of seamounts are shown in Figure 4-1-2. Topographic features of the seamounts are as follows;

(SC01)

Peaked seamount, summit depth 1,200 - 1,590m, sea ridge running in the direction of NW-SE. This seamount is in the shape of two combined seamounts. For the sake of convenience it has been given the designations SC01(N) and SC01(S) by dividing it into north and south sides. The summit of SC01 is flat it has gentle slope of about 10° - 15°.

(SC02)

Small-scale peaked seamount, summit depth 1,040m. The long axis extends N-S. A small seamount of 1,685m stands at the northern part. Another small seamount of 1,920m stands at the northeastward 10 mile point. A 300 m pinnacle (relative height) is on the top. The summit is flat and the inclination of slope is 15° - 20°.

(SC03)

Small scaled peaked seamount, summit depth 1,140m.

Another seamount of 1,520m stands 20 miles to the southwest of this seamount. According to charts, Merlin Seamount (1,370m) should stand in between these two seamounts. A shortage of sounding data when the chart was drawn may have caused the two to be taken as one seamount. The summit of SC03 is flat and a dike-shaped pinnacle of relative height 100m is observed.

(SC04)

Summit depth is 805m, the most shallow seamount in the survey area. Morphology in plan view is star-shaped, with flat ground at around 1,600m. The inclination of slope is 20° - 25°.

(SC05) --- Flint Island

According to the classification of coral reefs, Flint Island belongs to the table reef. A long and narrow seamount in NW-SE direction, it is connected to a small seamount of 2,970m, 20 miles to the northwest. An uncharted seamount of 1,970m is observed 20 miles west.

(SC06)

Small scaled peaked seamount, summit depth 1,130m, with narrow summit and no pinnacle. The inclination of slope is about 20°.

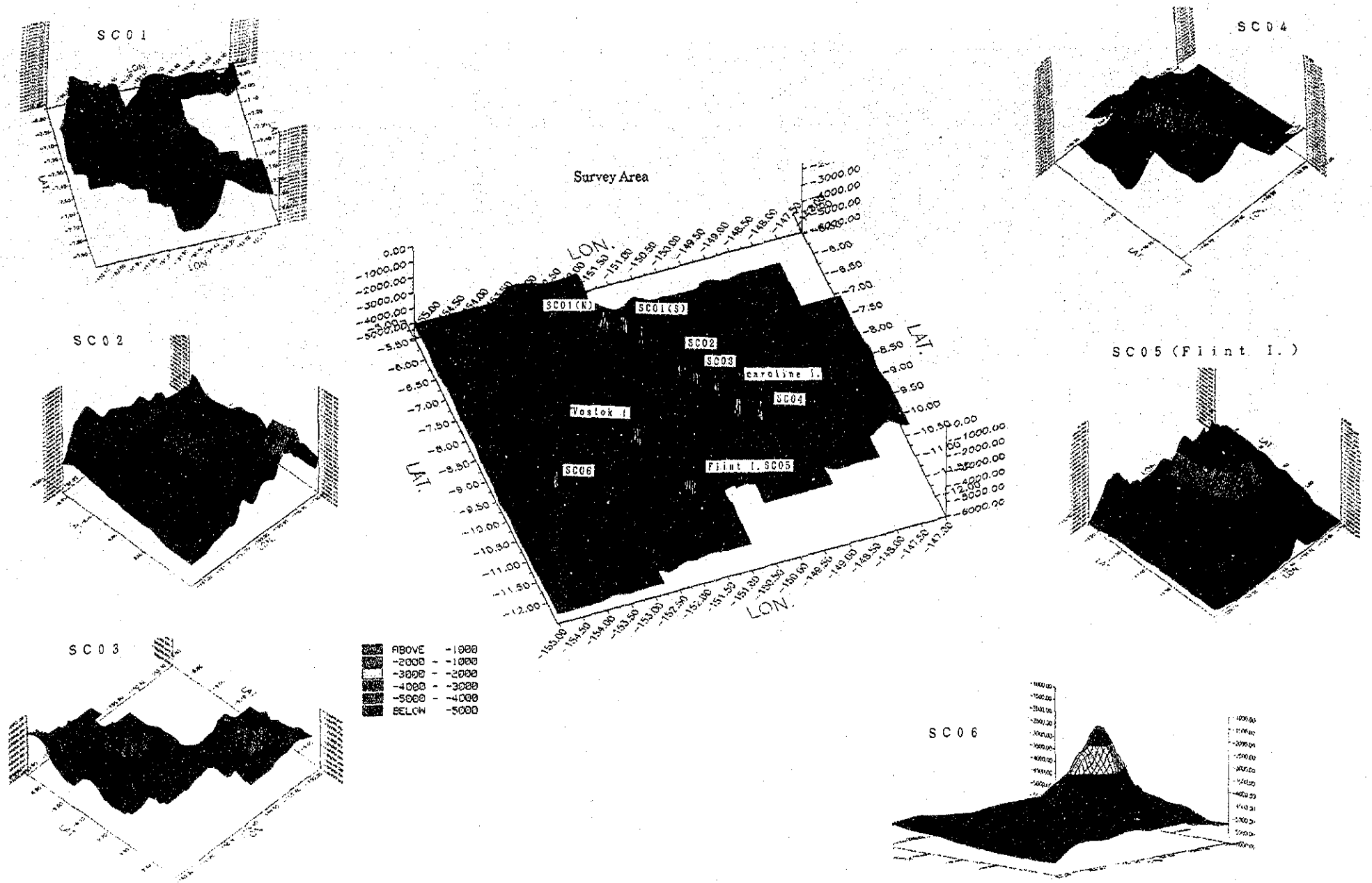

Figure 4-1-2 Bird's Eye Views of Seamounts

Table 4-1-4 Topographic Features of Individual Seamounts (1)

Sea-mount	Macroscopic Topography	Microscopic Topography
SC01 (N)	Location 7°20' S, 151°52' W Type peaked seamount Scale*1 16×47 km Range of Water Depth 1,590~5,000m Size of Top 5×5 km Inclination of Slope Upper part 11° (1° - 20°) Middle part 9° (0° - 29°) Lower part 5° (0° - 17°) Others: Sea ridges are connected in NW-SE direction. Flat summit	SBP Data T-type with about 20m transparent layer on the summit but locally, O-H type is prominently observed Area (Water depth) less than 2,400 m 141 km^2 summit 62 km^2 slope 79 km^2 Others
SC01 (S)	Location 7°33' S, 151°32' W Type peaked seamount Scale*1 17×42 km Range of Water Depth 1,200~5,000m Size of Top 5×5 km Inclination of Slope Upper part 13° (1° - 24°) Middle part 10° (0° - 22°) Lower part 6° (0° - 19°) Others: Sea ridges are connected in NW-SE direction. Flat summit	SBP Data T-type with about 20m transparent layer on the summit but locally, O-H type is prominently observed Area (Water depth) less than 2,400 m 179 km^2 summit 97 km^2 slope 82 km^2 Others: Pinnacle of 400m relative height on the summit
SC02	Location 8°52' S, 150°57.5' W Type peaked seamount Scale*1 10×24 km Range of Water Depth 1,040~4,000m Size of Top 5×5 km Inclination of Slope Upper part 14° (1° - 29°) Middle part 12° (0° - 29°) Lower part 6° (0° - 40°) Others: Direction of major axis N-S small seamount of 1,685m in the north. Flat summit	SBP Data T-type with 10-40m transparent layer on the summit but locally, O-H type is prominently observed Area (Water depth) less than 2,400 m 217 km^2 summit 25 km^2 slope 192 km^2 Others: Pinnacle of 300m relative height on the summit

Table 4-1-4 Topographic Features of Individual Seamounts (2)

Seamount	Macroscopic Topography	Microscopic Topography
SC03	Location 9°05' S, 150°43' W Type peaked seamount Scale*1 15×15 km Range of Water Depth 1,140~4,500m Size of Top 4×4 km Inclination of Slope Upper part 14° (1° - 26°) Middle part 12° (0° - 28°) Lower part 6° (0° - 31°) Others: Flat summit	SBP Data T-type with about 70m transparent layer on the summit, O-H type at other parts Area (Water depth) less than 2,400 m 219 km^2 summit 18 km^2 slope 201 km^2 Others: Dike shaped pinnacle of 100m relative height on the summit
SC04	Location 10°11' S, 149°49' W Type peaked seamount Scale*1 18×15 km Range of Water Depth 805~4,500m Size of Top 1×1 km Inclination of Slope Upper part 18° (2° - 34°) Middle part 16° (1° - 36°) Lower part 7° (0° - 33°) Others: Irregular shape, flat at around 1,600m	SBP Data T-type with 20-50m transparent layer on the south side flat of the summit, O-H type is prominent at other parts Area (Water depth) less than 2,400 m 145 km^2 summit 62 km^2 slope 83 km^2 Others:
SC05 Flint Island	Location 11°25' S, 151°50.0' W Type table reef Scale*1 28×10 km Range of Water Depth 0~4,500m Size of Top 4×1 km Inclination of Slope Upper part 17° (1° - 28°) Middle part 13° (1° - 24°) Lower part 4° (0° - 24°) Others: Direction of major axis NW-SE. Connected to a small seamount 20 miles to the northwest	SBP Data Side echo indicating slumping structure on the slope is observed Area (Water depth) less than 2,400 m 253 km^2 summit 1 km^2 slope 252 km^2 Others:

Table 4-1-4 Topographic Features of Individual Seamounts (3)

Sea-mount	Macroscopic Topography		Microscopic Topography		
SC06	Location	10°30' S, 154°12' W	SBP Data		
	Type	peaked seamount	O-H type only is observed, no T-type		
	Scale*1	15×12 km			
	Range of Water Depth	1,130~4,700m			
	Size of Top	2×2 km			
	Inclination of Slope		Area (Water depth)		
	Upper part	18° (5° - 25°)	less than	2,400 m	58 km^2
	Middle part	17° (5° - 25°)		summit	6 km^2
	Lower part	4° (0° - 24°)		slope	52 km^2
	Others:		Others:		

*1. range of half depth between top and basement for subdivision of slope refer Table 4-1-3.

3) Classification by SBP Type

Three SBP types are observed at the target seamounts. Typical examples of them are shown in Figure 4-1-3.

T-type: transparent layers on the upper parts.

O-type: composed of opaque layers.

H-type: composed of hyperbolic curve caused by diffraction.

T-type sediments are observed only locally on the summits of SC01-SC04. Transparent layers are as thin as 10-70m.

On the other hand, O-type and H-type sediments are prominently observed at the summits and slopes of every seamount. T-type with transparent layers 50-100m thick is usually observed on the summit of a typical guyot, but in this sea area, T-type is distributed only locally even on the seamounts (SC01, 02, 03) with rather flat summits. Thus the characteristics of peaked seamounts are recognised here. The zones with T-type sediments correspond to uncongealed sediments while the zones with O-type correspond to cobalt crusts, limestone and basalt. H-type reflects the influence of topography and according to the differences of transparency, the sediments would change to T-type or O-type.

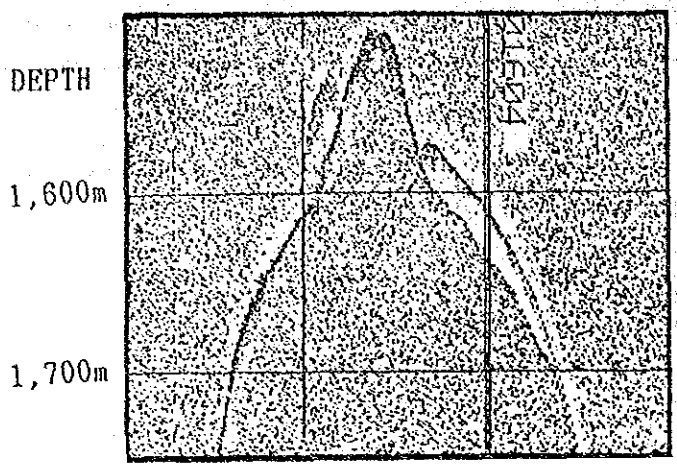

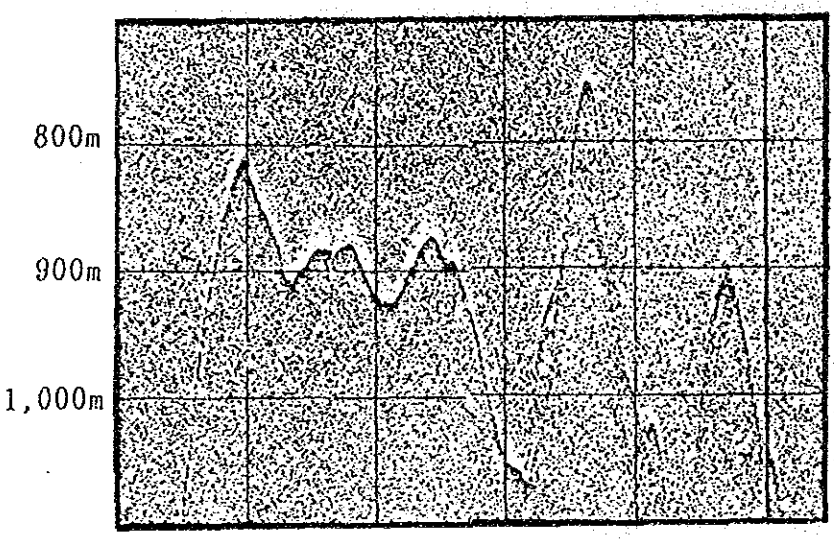

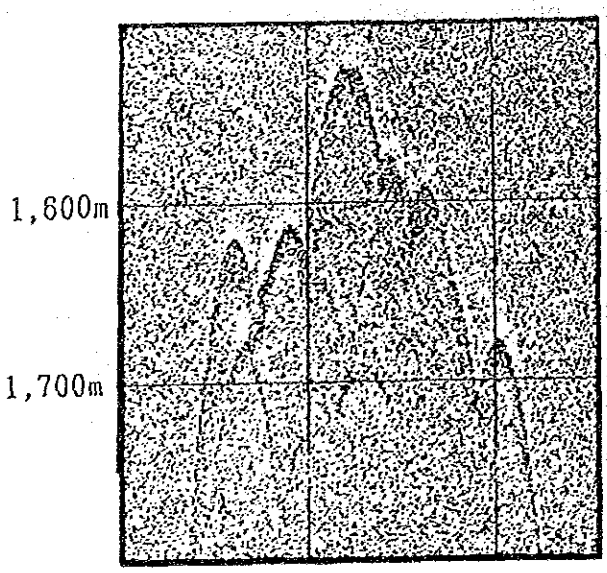

Figure 4-1-3 SBP Profile of Seamounts

4-2 Seamount Geology

1) Geology

The six surveyed seamounts are classified into peaked seamounts (SC01-SC04, SC06) and table reef (SC05: Flint Island) according to their morphology.

From the results of sampling by dredging and FDC survey, it is found that the seamounts are composed of principal rocks such as basalt, hyaloclastite, pyroclastic rocks, paleo-sediments, and limestone widely covered by foraminifera, unskeletal sediments of foraminifera.

Outline of Geology of Individual Seamounts is shown in Table 4-2-1. Geology of each seamount and distribution of cobalt are shown in Annexed Figure 21 (1) - (6).

It is presumed that rocks such as basalt, hyaloclastite, pyroclastics, etc., are forming the basement complex of each seamount. These rocks were collected widely ranging from the summit to the middle part of the slopes of the peaked seamounts. A large amount of basalt, hyaloclastite, pyroclastic rocks, etc., were collected from depths below 1,200m of the table reef Flint Island. Usually, basalt foams and is rich in vesicles, therefore, it is inferable that the seamounts were formed in shallower seas than present depths (some parts might have been formed on shore?).

Paleo-sediments are composed of siltstone, limestone, sandstone etc., and they were collected from the northwestern slopes and southeastern slopes of the SC04 seamounts.

Limestone is one of the principal rocks composing the seamounts and is prominently distributed on the summits or the upper part of slopes of the seamounts. At the upper part of the slope (shallower than 1,200m) of Flint Island, only limestone is collected. There are two kinds of limestone, one is composed of hermetic coral and the other is composed of microfossils such as foraminifera, calcareous algae, etc. The former was collected only from the Flint Island table reef. The type of crust grown on the surface is the coating type only.
On the other hand, the latter was collected from every seamount. Most of the latter exist as host rocks or the cores of crust type crusts, slab type crusts, etc., and has already decomposed into phosphate.

Phosphorite is sampled from every seamount, and it forms the matrix of hyaloclastite, pyroclastics, etc., or replaces limestone.

Non-skeletal sediments are composed of foraminifera ooze and prominently distributed of such topography as summit planations or slope-terraces.

Table 4-2-1 Geology of Individual Seamounts (1)

Seamount	Sampling Data
SC01	Lithology: • Basalt, Hyaloclastite • Pyroclastic rock • Limestone • Unskeletal sediments
	Characteristics: • Basalt and hyaloclastite are prominent. Basalt contains phenocryst of unidentified species. Pyroclastic is composed of basalt, its matrix is replaced by phosphorite. • Basalt boulders are sampled, morphology of boulder is presumed to be the effect of the water's edge. • Limestone is composed of hermatic sediments containing foraminifera fossils. Limestone is decomposed into phosphorite in varying degrees. • Few amount of crusts and rocks are collected from the summit and presumed to be prominent in unskeletal sediments. • Rich in boulder type accompanied with slab type and crust type.
SC02	Lithology: • Basalt, Hyaloclastite • Pyroclastic rock • Limesotne • Unskeletal sediments
	Characteristics: • Basalt and hyaloclastite are prominent. Basalt are mostly foamed and in almond shape. Pyroclastic is composed of basalt, its matrix is replaced by phosphorite. • Limestone is composed of hermatic sediments containing foraminifera fossils. Pure limestone is existing but, most of it is decomposed into phosphorite. • Only limestone was collected from the depth of less than 1,500 m. • Basalt is prominently distributed at the western part of seamount. • Mostly are crust type accompanied with slab type, cobble type and nodule type.

Table 4-2-1 Geology of Individual Seamounts (2)

Seamount	Sampling Data
SC03	Lithology: • Basalt, Hyaloclastite • Pyroclastic rock • Limestone • Unskeletal sediments
	Characteristics: • Prominent in limesotne. Limestone is composed of hermatic coral containing foraminifera and bivalve fossils. Limestone is decomposed into phosphorite in varying degrees. Plently of pores caused by benthos. • Several species of basalt such as non-phenocryst, phenocryst of proxene, etc.. A large amount of foamed basalt boulders in almond shape were collected from the southern slope in the depth of about 2,000 m. • Fine-grained of stratified tuff was collected at the northwestern and southeastern part of seamount. • Plenty of crust type accompanied with nodule type and cobble type.
SC04	Lithology: • Basalt, Hyaloclastite • Pyroclastic rock • Paleo-sediments • Limestone • Unskeletal sediments
	Characteristics: • Prominent in limesotne. Limestone is composed of hermatic sediments containing foraminifera fossils, bivalve fossils, snail fossils, etc.. Some basalt contains breccia. Most limestone is decomposed into phosphorite in varying degrees. • Only limestone was collected at the summit (depth of less than 1,700 m). • Fine-grained stratified tuff was collected at the western part and eastern part of seamount. • Fine-grained brown psammite (some calcareous) was collected at the southwestern and northern part of seamount. • Plently of crust type accompanied with cobble type, slab type and nodule type.

Table 4-2-1 Geology of Individual Seamounts (3)

Seamount	Sampling Data
SC05	Lithology: · Basalt, Hyaloclastite · Pyroclastic rock · Limestone · Unskeletal sediments
	Characteristics: · Prominent in limesotne. Limestone is composed of hermatic sediments containing fossils of hermatic coral, foraminifera, bivalve, etc.. Limestone is decomposed into phosphorite in varying degrees. Plenty of pores caused by benthos. · Basalt is mostly foamed and almond-shaped. · Only limesone was collected in the depth of less than 1,200m. · Development of crust is bad, most crusts are coating type with the thickness of less than 1 mm. Coating type and crust type are observed as depth increase.
SC06	Lithology: · Basalt, Hyaloclastite · Pyroclastic rock · Limestone · Unskeletal sediments
	Characteristics: · Prominent in Basalt and Hyaloclastite. Most of basalt is foamed and almond-shaped. · Basalt and pyroclastic rock collected at the western part of seamount contains big phenocryst of pyroxene (maximum dia. is about 1 cm). · Limestone is composed of hermatic sediments containing fossils of foraminifera, etc.. Most of limestone is decomposed into phosphorite in varying degrees. Limestone is fewer compared with other seamounts. · Rich in crust type accompaning slab type.

According to FDC observation, ripple marks are recognized on the non-skeletal sediments distributed at summits or the upper part of slopes. Trends of bottom streamline flow estimated from the ripple marks are as follows;

Seamount SC02 : SW → NE
SC03 : WNW → ESE ~ NW → SE
SC04 : N → S ~ NNW → SSE

However, ripple marks are not recognized in the deeper zones due to the transition of non-skeletal sediments into slumping sediments.

2) Description of Substrates

(1) Unaided eye and microscopic observation

13 samples were selected from the sampled rocks and thin sections were made for observation by polarization-microscope. The samples observed by microscope are also experimented with by X-ray diffraction for identifying their mineral content. Photographs of typical rocks are shown in Figure 4-2-1. Name of rocks identified by microscopic observation and the result of X-ray diffraction are shown in Table 4-2-2. Microphotographs are shown in Figure 4-2-2.

① Basalt

(Unaided-eye characteristics)

From the texture and assemblage of phenocrysts, existence of plural species of basalt is presumed. Most of the samples are altered to clay or phosphate, though the alteration is in varying degrees. However, there are some samples with gas seepage indicating recent activity. Most of the samples have amygdaloidal structure with plenty of vesicles, and those vesicles are usually filled with zeolite and calcite. Some samples are presumed to be pillow lava in the ellipsoidal morphology. This fact is also confirmed by the FDC observation.

(Microscopic observation)

As phenocryst, there are plagioclase, augite and titanaugite, but due to heavy alteration of minerals (montmorillonite was detected by X-ray diffraction), it is difficult to identify the names of rocks.

Groundmass is composed of plagioclass, augite, glass, opaque minerals, etc. Opaque minerals coexist with glass and most of them are altered into goethite. Groundmass shows intersertal texture, but normally, this kind of

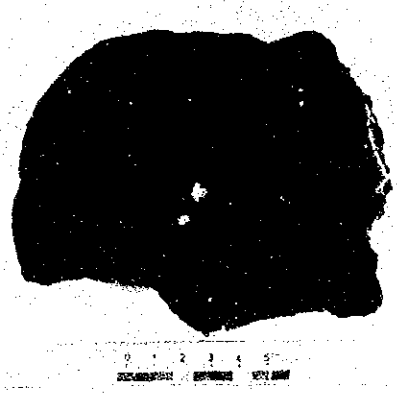

(a) Basalt (ST. No. 89SC04AD06)

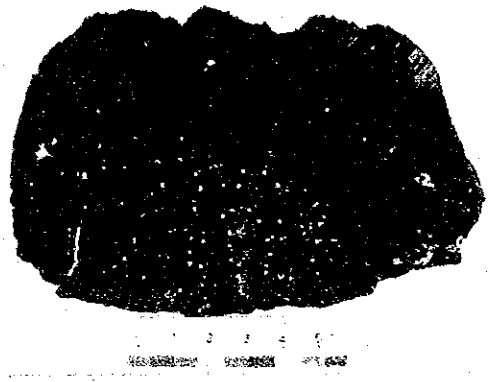

(b) Basalt (ST. No. 89SC02AD04)

(c) Tuff Breccia (ST. No. 89SC04AD07)

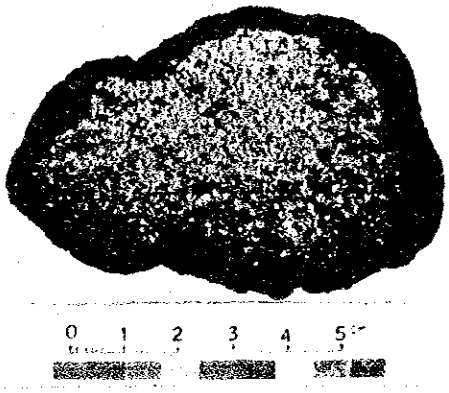

(d) Hyaloclastite (ST. No. 89SC01AD03)

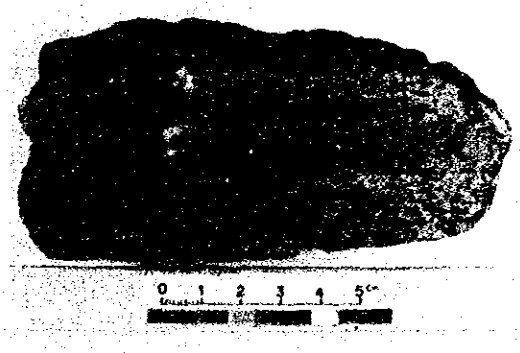

(e) Tuff (ST. No. 89SC03AD01)

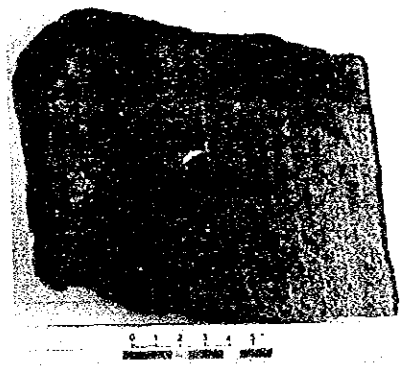

(f) Tuff (ST. No. 89SC04AD06)

Figure 4-2-1 Photos of Representative Rocks (1)

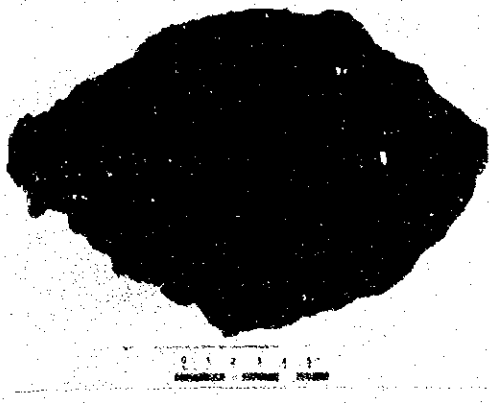

(g) Sandstone (ST. No. 89SC04AD05)

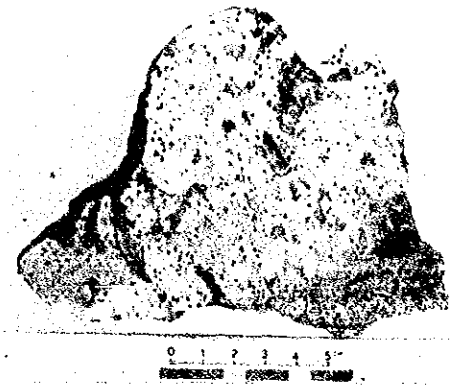

(h) Limestone (ST. No. 89SC03AD01)

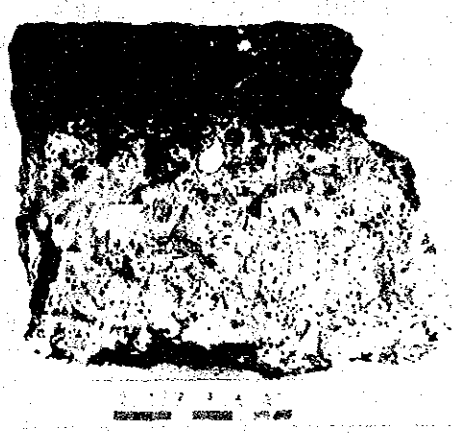

(i) Limestone (ST. No. 89SC01AD03)

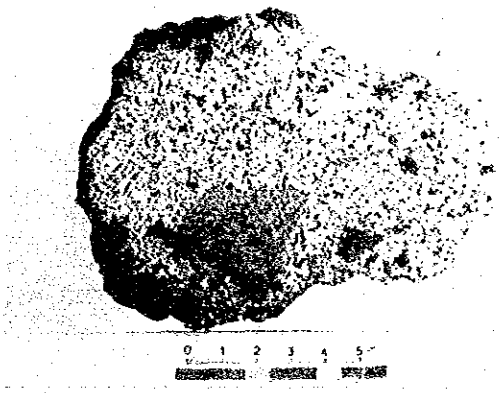

(j) Calcareous Sandstone
(ST. No. 89SC04AD09)

(k) Phosphorite (ST. No. 89SC04AD03)

Figure 4-2-1 Photos of Representative Rocks (2)

Table 4-2-2 Results of X-ray Diffraction Analysis of Rocks

No.	Sample No.	Rocks*1	Pl	Mo	Ka	Ph	Ap	Cal	Goe
1	89SC02AD04	Amygdaloidal Basalt	⫩	+				+	
2	89SC04AD06 (C)	Amygdaloidal Basalt	⫩	±					
3	89SC04AD09 (A)	Basalt	⫩						
4	89SC05AD05	Amygdaloidal titano augite Basalt	⫩						
5	89SC02AD06	Hyaloclastite with calcite in network						⫩	+
6	89SC03AD01	Hyaloclastite with montmorillonite alteration		⫫					
7	89SC04AD07 (A)	Hyaloclastite ~ Silicagel phase	⫩	+		+			
8	89SC06AD08	Altered Hyaloclastite ~ Silicagel phase		+		⫩			
9	89SC02AD02	〃 〃		±	±	+	+		
10	89SC02AD02 (A)	Carbonate rock with microfossils					+	+	
11	89SC02AD08	Phosphorite with limonite					⫫		
12	89SC04AD03 (A)	Porous siliceous material with microfossils		±		+			

*1 Determined by microscopic observation

Legend Pl : Plagioclase Mo : Montmorillonite Ka : Kaolinite Ph : Phillipsite
Ap : Apatite Cal : Calcite Goe : Goethite
⫫ : Reflection is very strong ⫩ : Reflection is strong
+ : Reflection is weak ± : Reflection is very weak or obscure
Cu-monochrometer, 35 kV, 20 mA

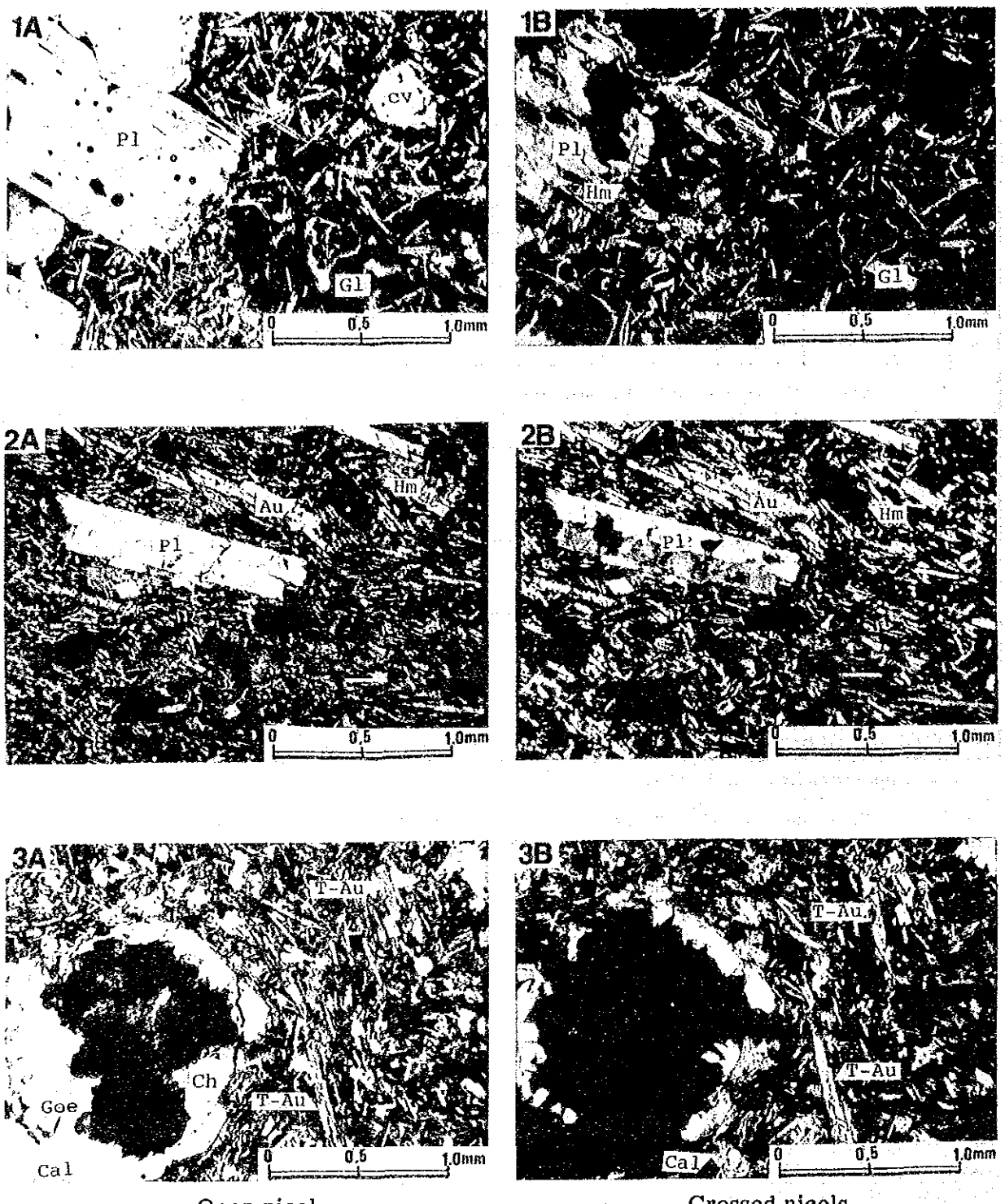

Open nicol

Crossed nicols

Legend Pl : Plagioclase Au : Augite T-Au : Tinano Augite Ch : Chlorite
Cal : Calcite Hm : Hematite Goe : Goethite Gl : Glass Cv : Cavity

1A, B : 89SC04AD06 (C) Amygdaloidal Basalt
2A, B : 89SC04AD09 (A) Basalt
3A, B : 89SC05AD05 Amygdaloidal Titano Augite Basalt

Figure 4-2-2 Microscopic Photos of Substrates (1)

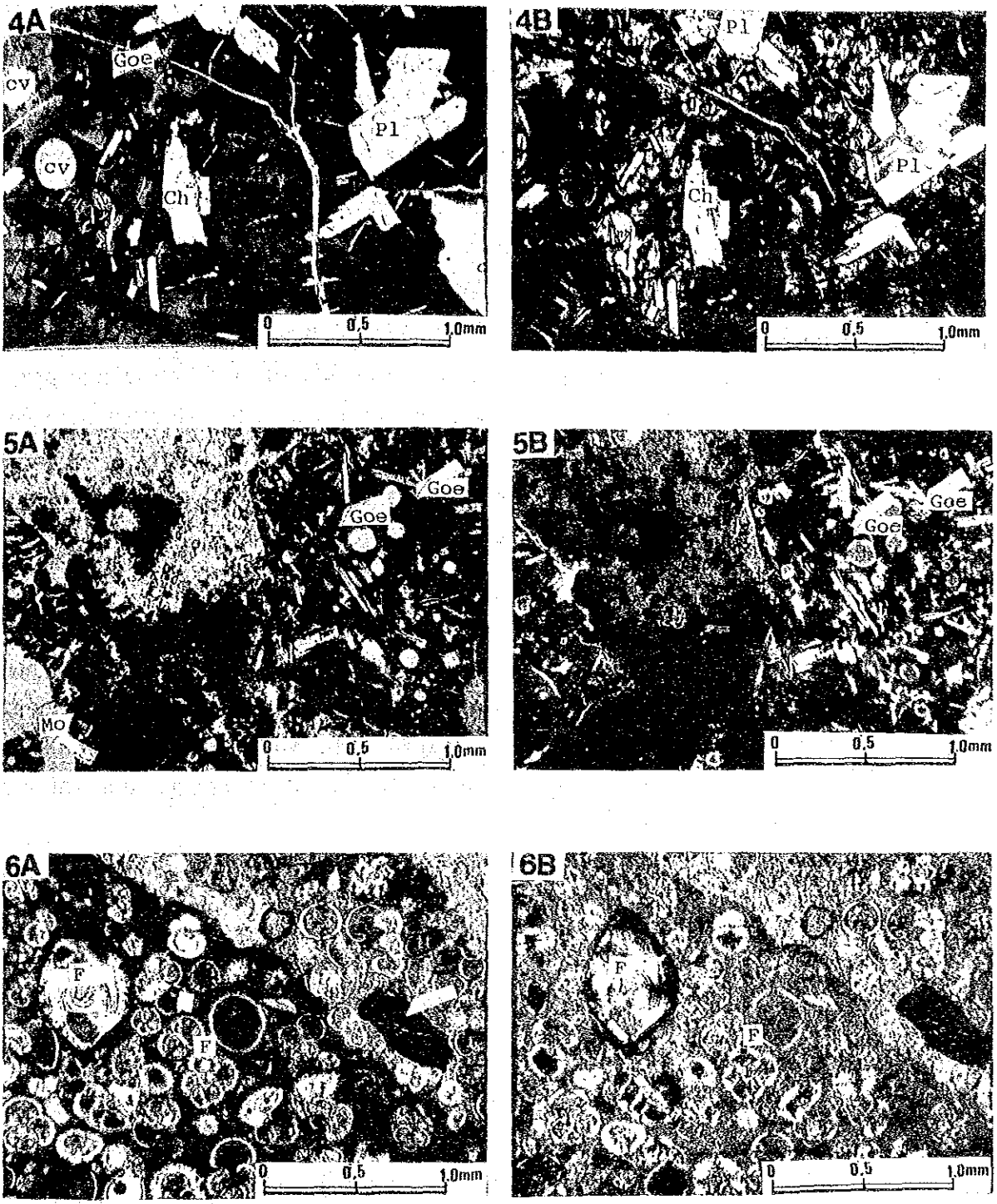

Open nicol

Crossed nicols

Legend Pl : Plagioclase Ch : Chlorite Mo : Montmorillonite Goe : Goethite
F : Fossil Cv : Cavity

4A, B : 89SC04AD07 (A) Hyaloclastite ~ Silica Gel phase
5A, B : 89SC02AD02 Altered Hyaloclastite ~ Silica Gel phase
6A, B : 89SC02AD02 (A) Carbonate rock with micro Fossils

Figure 4-2-2 Microscopic Photos of Substrates (2)

texture is not recognized among the quenched textures, so it might have been formed on shore.

Normally, vesicles are filled with calcite but some are filled with zeolite (phillipsite?).

② Hyaloclastite

(Unaided-eye Characteristics)

Hyaloclastite was sampled widely from the summits and the middle parts of slopes together with basalt and pyroclastics. Classification between hyaloclastite and pyroclastics was made by identifying their breccia was essential or accidental. However, owing to the alteration of matrix into clay or phosphate, many of them are unidentifiable.

(Microscopic observation)

Hyaloclastite is prominent in hyaline texture. Breccia is composed of fragments of basalt lava accompanied with phenocryst of plagioclase and augite. Matrix is composed of non-crystalline silica gel and micro-grained chalcedony but mostly are altered into such clay minerals as montmorillonite or altered to phosphate. Most of opaque mineral are altered to goethite.

Plagioclase, montmorillonite, kaolinite, phillipsite, calcite and goethite are detected by X-ray diffraction.

③ Pyroclastic rock

(Unaided-eye Characteristics)

Pyroclastic rock is composed of tuff breccia, tuff, etc. accompanied with basalt and hyaloclastite and was widely sampled from the summits and the middle parts of seamount slopes.

Tuff breccia is composed of breccia and subbreccia of basalt, but the matrix is mostly decomposed into clay or phosphate.

The color of tuff breccia from the SC03 and the SC04 is yellowish green. Fine-grained stratified tuff was sampled from these two seamounts. The tuff collected from the SC04 is contained in the limestone as pebbles. This shows that some of the tuff had been formed by activities which occurred

before the limestone formation.

④ Paleo-Sediments

(Unaided-eye characteristics)

The color of the Paleo-sediments is dark brown and yellowish white. Composed of calcareous sandstone mixed with a small amount of tuff. Paleo-sediments were sampled from northwestern slope and south-eastern slope of the SC04.

⑤ Limestone

(Unaided-eye characteristics)

Two kinds of limestone were collected from the survey area, one originates in hermetic coral and the other in calcareous algae. Limestone originating in hermetic coral is a relatively compact one and the degree of alteration into phosphate is not so great. On the other hand, the latter type is soft with holes bored by bottom fauna and strongly decomposed into phosphate.

The identification of limestone and phosphorite was carried out on board by the method of hydrochloric acid foaming.

(Microscopic Observation)

Limestone originating in foraminifera contains a large amount of foraminifera fossils (mostly the diameter of 0.5 - 0.1mm) and a small amount of diatom fossils. Although in varing degrees, they are decomposed into phosphate, and according to the degrees of decomposition, they are classified into limestone (weakly decomposed) and phosphorite (strongly decomposed).

Containing a small amount of pyroclastic rock fragments, the fragments are already decomposed into goethite.

⑥ Phosphorite

(Unaided-eye characteristics)

The color is light brown and the grain is fine, it is presumed to be formed by replacing matrix of hyaloclastite, matrix of pyroclastic rock and limestone. The border of rock and crust has a tendency to be strongly

phosphated. Permeation of manganese oxide into phosphorite and the existence of paleo-crust fragments inside phosphorite are observed.

(Microscopic observation)

Phosphorite originating in limestone contains a large amount of microfossils such as foraminifera. Some of the microfossils still retain their original texture but mostly are completely replaced by phosphorite.

Apatite and calcite are detected by X-ray diffraction.

(2) X-ray Diffraction

Five samples were selected from among materials adhered to crusts, alteration zones of host rocks and adherents of host rocks to undergo the X-ray diffraction test. The result of X-ray diffraction is shown in table 4-2-3. The diffraction charts are shown in Figure 4-2-3.

Samples No. 1, No. 2 and No. 5 are clay, light brown in colour, that filled the pores and crevices of the host rocks. They are viscous and smooth to the touch. Apatite, calcite and peak of aragonite are detected by X-ray diffraction.

Sample No. 3 is a white-coloured impurity found between rock and crust. Sample No. 4 is a white-coloured material in the veined host rocks. Apatite and peak of calcite are detected by X-ray diffraction. These samples are considered to be mainly composed of phosphorite.

(3) Chemical Analysis

Five samples were selected from among materials related to crust and host rocks for chemical analysis. The result of chemical analysis is shown in Table 4-2-4. Analyzed samples are the same species as the samples subjected to X-ray diffraction.

Samples No. 1, No. 2 and No. 5 are clay, light brown in color. They contain large amount of CaO (40.0 - 54.3%) together with SiO_2, Al_2O_3, Na_2O and P_2O_5, and are especially rich in P_2O_5 (0.2 - 8.8%).

Sample No. 3 and Sample No. 4 are a white-coloured material. Sample No. 3 was found in between crust and host rock. Sample No. 4 was mingled in the host rock as veins. They are composed of a large amount of CaO (53.7 -

Table 4-2-3 Results of X-ray Diffraction Analysis of Clayish Materials

No.	Sample No.	Ap	Cal	Ar	Remarks
1	89SC01AD03	±	⫫		Pale brown clay (Foraminifera ooze)
2	89SC02AD02	±	⫫		Pale brown clay (Foraminifera ooze)
3	89SC03AD02 (A)	+	⫩		Phosphorite layer among substrate and crust
4	89SC04AD03 (A)	⫩	±		Phosphorite
5	89SC05AD08 (A)		⫫	±	Pale brown clay (Foraminifera ooze)

Legend Ap : Apatite Cal : Calcite Ar : Aragonite
⫫ : Reflection is very strong ⫩ : Reflection is strong
+ : Reflection is weak ± : Reflection is very weak or obscure
Cu-Monochrometer, 45kV, 20mA

Table 4-2-4 Results of Chemical Analysis of Clayish Materials

(%)

No.	Sample No.	SiO_2	TiO_2	Al_2O_3	Fe_2O_3	FeO	MnO	MgO	CaO
1	89SC01AD03	8.89	0.44	3.52	3.99	0.25	1.48	0.71	38.97
2	89SC02AD02	0.40	0.05	0.17	0.17	0.25	0.10	0.39	54.36
3	89SC03AD02 (A)	0.56	0.04	0.13	0.27	0.13	0.07	0.41	53.94
4	89SC04AD03 (A)	0.28	0.02	0.05	0.13	0.25	0.16	0.63	53.72
5	89SC05AD08 (A)	0.86	0.03	0.11	0.13	0.13	0.05	0.45	51.94

No.	BaO	Na_2O	K_2O	P_2O_5	Ig-loss	Remarks
1	0.09	1.82	0.41	1.35	37.66	Pale brown clay (Foraminifera ooze)
2	0.06	0.91	0.02	6.30	36.93	Pale brown clay (Foraminifera ooze)
3	0.42	0.55	0.01	8.75	34.22	Phosphorite layer among substrate and crust
4	0.02	1.49	0.02	31.30	11.56	Phosphorite
5	0.16	1.25	0.02	0.18	44.44	Pale brown clay (Foraminifera ooze)

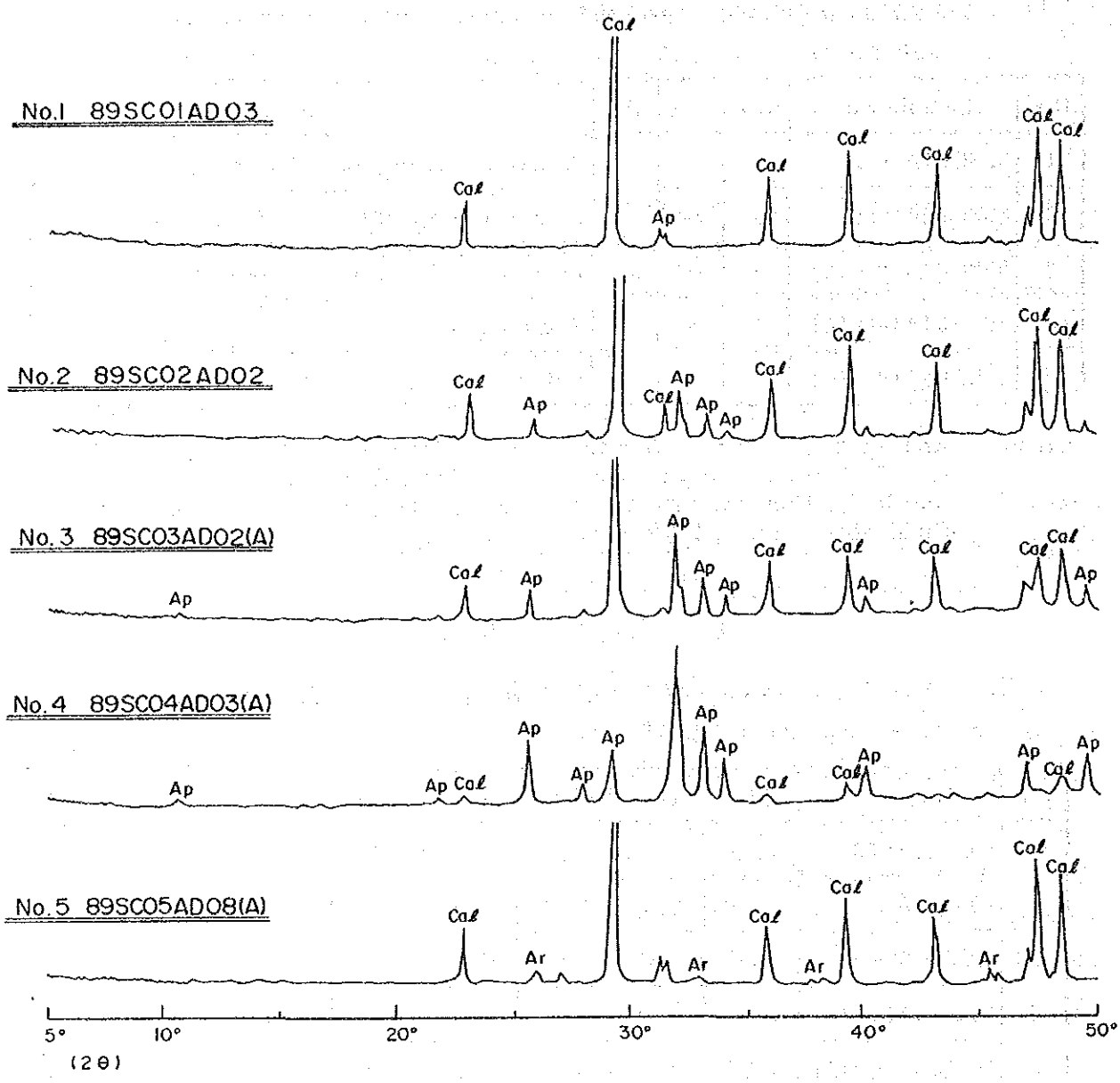

Legend Ap : Apatite Cal : Calcite Ar : Aragonite

Figure 4-2-3 X-ray Diffraction Patterns of Clayish Materials

53.9%) and P_2O_5 (8.8 - 31.3%) accompanied by a small amount of SiO_2, MgO, Na_2O, etc.

Apatite, calcite and aragonite are detected by X-ray diffraction. The analysis value of P_2O_5 is considered to be apatite contained in clay. From the external appearance, clay is considered to have originated in foraminifera ooze that filled the pores and crevices of rocks. Alteration process of foraminifera ooze into clay containing P_2O_5 is not clear. However, from the results of X-ray diffraction and chemical analysis, following presumption is established: The ooze decomposed from foraminifera fossils mixed with weathered soil decomposed from basalt and became light brown clay. During the process $CaCO_3$ originated in foraminifera ooze, SiO_2, Al_2O_3, Na_2O, etc., originated in basalt and P ions adhered from seawater. As for the apatite ($Ca_5(PO_4)$ (OH F Cl), it is assumed that P ions crystallized in the process of diagenesis. Then the clay hardened in the pores and crevices to become phosphorite.

3) Age Determination

One of the freshest samples was selected from the basalt collected from the seamounts to determine the age of the seamounts. Age determination is implemented by K-Ar (whole rock) Method. The selected sample was basalt collected from the lower part of the slope of the SC04 at the water depth of 3,115m. According to the microscopic observation, this sample is fine-grained basalt containing phenocryst of anorthosite. Although the groundmass hyaline was already decomposed into smectite and non-ferrous minerals such as pyroxene were decomposed (alteration into smectite and hematite), the degree of alteration proved to be sufficient to measure the age.

The result is as follows:

Sample Number	89SC04AD06
Original Radioactive of ^{40}Ar	0.193 ± 0.008 ($\times 10^{-5}$ cc/g)
K-Ar age	36.2 ± 19 (Ma)

The result of this age measurement suggests the age of SC04 basalt as the Oligocene period.

4-3 Mode of Cobalt Crust Occurrences

1) Type

The occurrence and morphology of the cobalt crusts observed by unaided eye are classified into several groups as listed in Table 4-3-1. On the other hand, the samples collected from the survey area and the cobalt crusts observed by the FDC are classified into seven groups. (Figure 4-3-1, 4-3-2)

① Crust type
② Slab type
③ Pavement type
④ Massive type
⑤ Cobble type
⑥ Nodule type
⑦ Coating type

Crust type: The crust develops on the surface of rocks and in the survey area this type is recognised on rocks such as basalt, sedimentary rocks, limestone, etc.. This type is distributed in the whole survey area from the top to the mid-slope of the seamounts and it shows the highest frequency in occurrence among the seven types. (Table 4-3-2)

Slab type: The crust covers the top and the bottom of sample. Usually scattered on the sea floor.

Pavement type: Crust type, slab type or cobble type crusts develop on the whole surface in pavement-like form. Samples of this type on board are usually classified into the crust type, slab type or cobble type.

Cobble type and Nodule type: Crusts develop over rock and the mode of occurrence is like that of manganese nodules. Widely distributed on the sea floor where there are sediments on the summit or slope.

Coating type: The crust coating on rocks with a thickness of only a few mm. Mostly unable to analyze.

Massive type: Crusts in irregular shapes, rare in this survey area.

Table 4-3-1 Classification of Types of Cobalt Crusts

Group	Type	Characteristics and distribution
Crust type group	Crust type	(Characteristics) The crust directly covers rocks such as basalt, pyroclastic rocks and sedimentary rocks. The crust is distributed continuously and presents large scale mode of occurrence. (Distribution) Prominent on every seamount Distributed on whole seamount from the summit to the lower part of slope.
	Slab type	(Characteristics) The crust is angular and flat-shaped, covering the whole surface. Partly exfoliated material is included. (Distribution) Seen on SC01, 02, 04, 06 with thick crusts.
	Pavement type	(Characteristics) This is a kind of crust shape. Crusts which were originally nodule or cobble shape combined with each other to form a pavement-like appearance. (Distribution) Seen on SC04.
Nodule type group	Massive type	(Characteristics) Crust develops over a core of rock fragments, external form is angular and irregular. Size varies. (Distribution) Rarely Seen.
	Cobble type	(Characteristics) Crust develops over a core of rock fragments, external form is rounded. The diameter is more than 10cm±. (Distribution) Seen on every seamount except SC05.
	Nodule type	(Characteristics) The mode of occurrence of this shape is the same as that of manganese nodules. This size ranges between pebble and fist-size (10cm ± in diameter) (Distribution) Seen on SC01, 02, 03 04.
Others	Film type or coating type	(Characteristics) The crust covers the substrate as thin film with a thickness of less than about 1 mm.

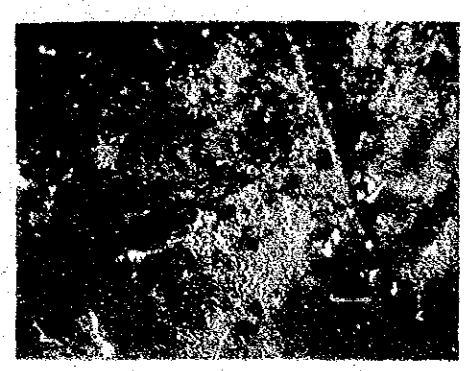

Crust type, SC04 seamount

Crust type, SC03 seamount

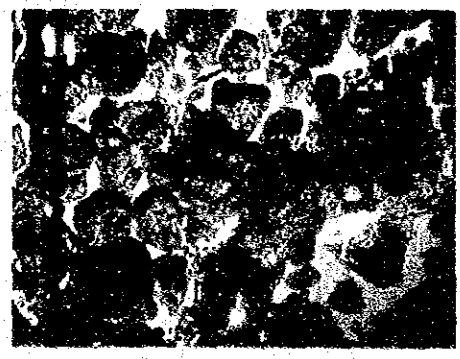

Cobble type, SC03 seamount

Cobble type, SC04 seamount

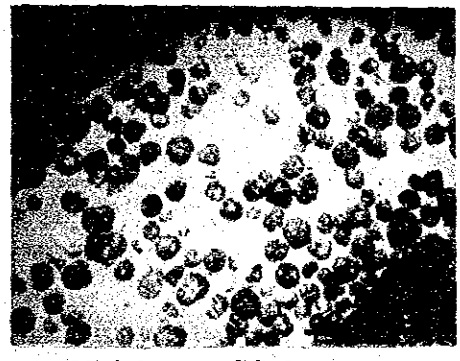

Nodule type, SC02 seamount

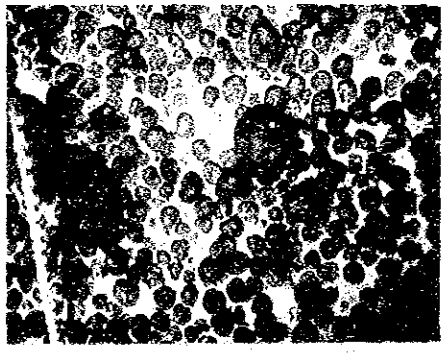

Nodule type, SC04 seamount

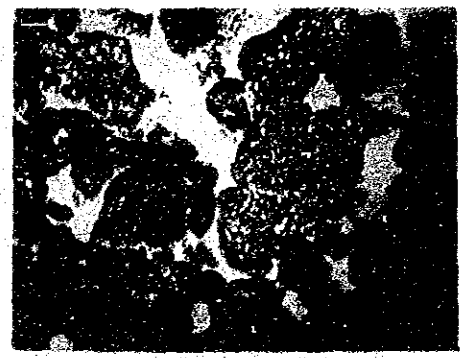

Slab type, SC04 seamount

Pavement type, SC04 seamount

Figure 4-3-1 Occurrence of Cobalt Crust (FDC photographs)

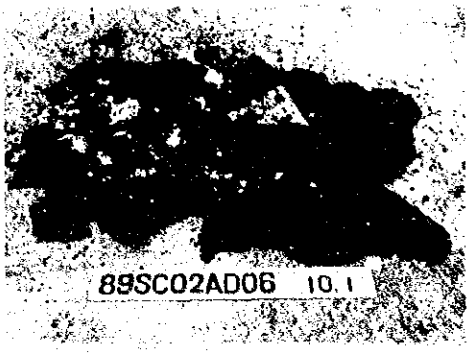

Crust type, 89SC02AD06

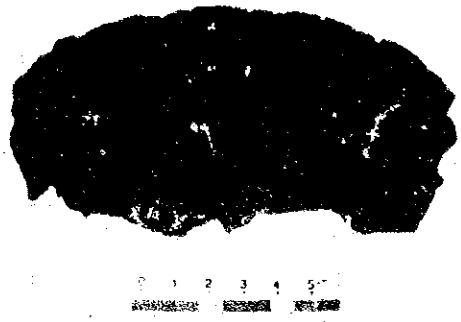

Same as left, Section

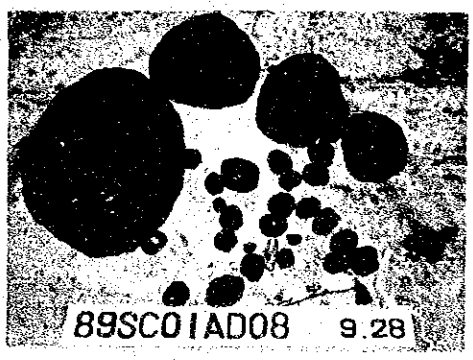

Cobble type, 89SC01AD08

Same as left, Section

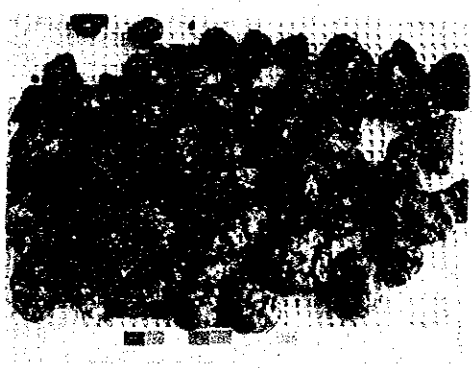

Nodule type, 89SC01AD03

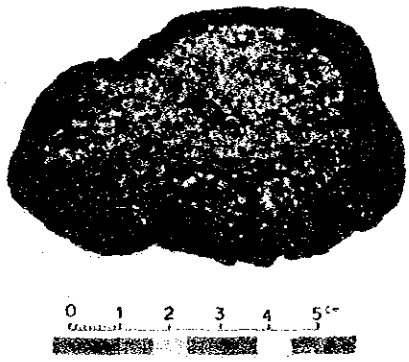

Same as left, Section

Slab type, 89SC04AD06

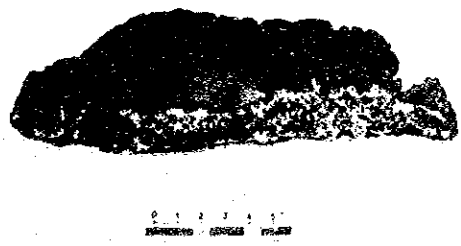

Same as left, Section

Figure 4-3-2 Representative Cobalt Crust Types (on Board)

Table 4-3-2 Appearance Rate by Type

Type	Number of analyzed samples	Frequency (%)
Crust type	79	67
Slab type	16	13
Pavement type	1	1
Cobble type	11	9
Nodule type	12	10
Total	119	100

2) Properties

Macroscopic properties, based on the observation at the sea floor by FDC and photographs, and microscopic properties of samples, observed by unaided eye and microscope, are as follows;

(1) Macroscopic Properties

Macroscopic properties of the crusts are classified into two types as follows;

① Considered to be developed from the manganese oxides that covered the surfaces of rocks such as basalt, hyaloclastite, limestone, etc..

② Considered to be developed from the microscopic manganese oxides core which had been fine particles of sediments or the remains of organisms.

Related sea bottom photographs are shown in Figures 4-3-3 and 4-3-4.

(a) The first case is observed at the neighborhood of summits, steep cliffs, basement rocks such as pinnacles and exposed rocks where it was difficult for sediments to settle. Figure 4-3-4 shows that in places where sediments were accumulate easily such as basins, gentle slopes, and slopes with slumping sediments, the mode of occurrences is poor. This illustrates how the topography of the sea floor influences occurrence.

(b) The second case shows cobalt crusts developed on the surface of sediments in the same mode of occurrence as manganese nodules. Favourable conditions for crusts to grow might be

① Short of supply of sediments
② Slow settling speed of sediments
③ Surficial sediments constantly washed by sea current

This illustrates how external elements such as sedimentation environment and sea currents etc., will influence the mode of occurrence. Figure 4-3-4 shows the different coverage of cobalt crusts according to the growing stages.

1 Top flat
Ripple mark observed on sediments

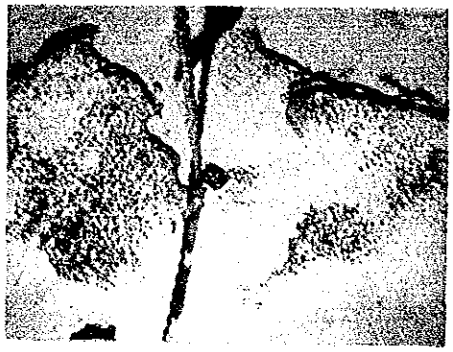

2 Top shoulder
Microtopography of stepwise slope

3 Upper slope
Outcrops of bedrock

4 Upper slope
Pillow lava (Basalt)

5 Middle slope
Mixture of rocks, pebbles, sediments

6 Lower slope
Slumping sediments

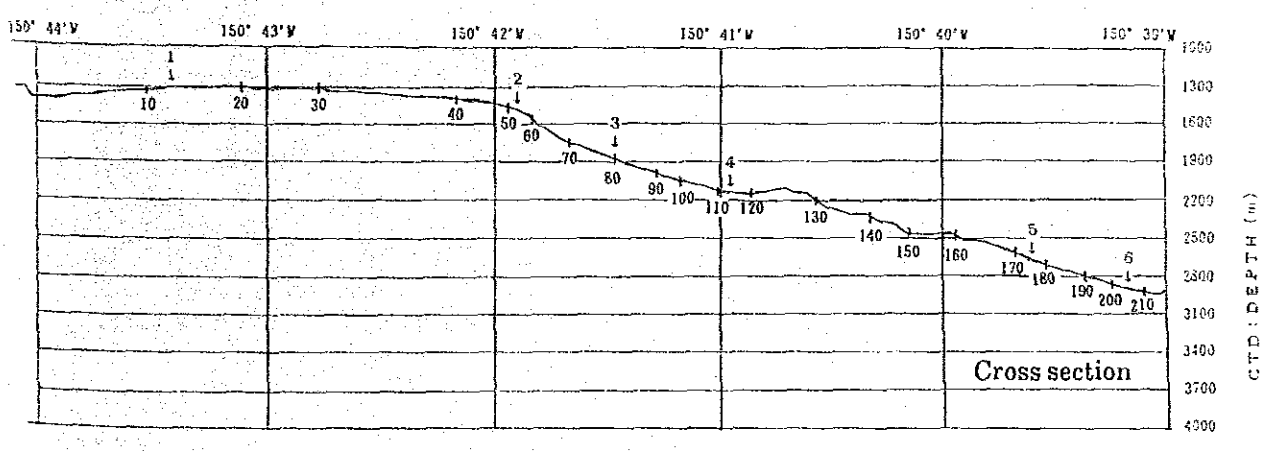

Figure 4-3-3 Topography of Seamount and Occurrence
(SC03 seamount, FDC photographs)

1 Coverage 2%

2 Coverage 12%

3 Coverage 19%

4 Coverage 26%

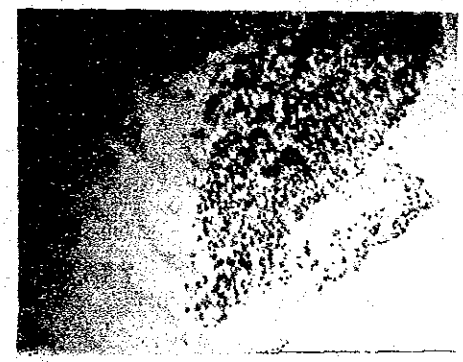

5 Coverage 32%

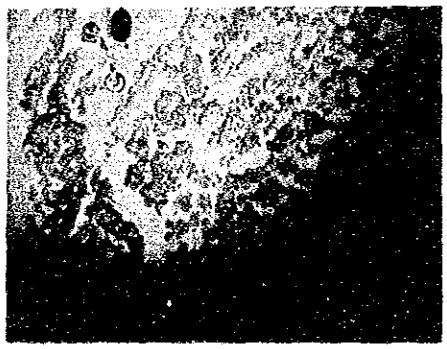

6 Coverage 56%

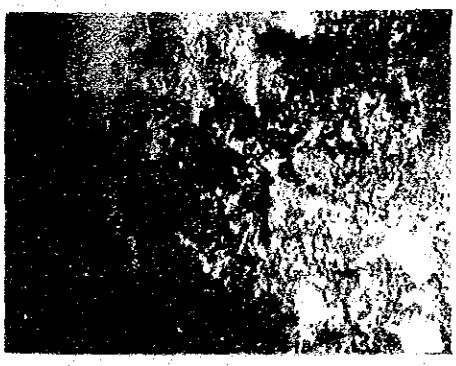

7 Coverage 85%

8 Coverage 95%

Figure 4-3-4 Coverage of Cobalt Crust (FDC photographs)

(2) Microscopic Properties

Following features of surficial structure and sectional structure are observed from the samples collected.

(Surficial Structure)

① Most of the samples have uneven surface. They are classified into two groups of Buddha-head type and Nipple type according to the size of the botryoidal structure by which the surface irregularities were caused. There are some samples with a smooth surface, but very few. (Figure 4-3-5)

(Sectional Structure)

② The samples of crust are classified into two groups according to the evenness of the sectional structure. One shows even structure through the whole thickness and the other different layers of varying fineness and porosity. (Figure 4-3-6)

In the case of double-layers, they show high porosity and contents of impurities in the outer shell; the surface is also rough. The apparent specific gravity of this layer is low. On the other hand, the inner shell is hard and fine. The apparent specific gravity is as high as 2.0 or more. There are some cases in which the outer and inner shells are fine but the inner shell is composed of a glasslike component.

③ In the case of crusts whose substrates are limestone, there are some examples showing that the inner limestone was replaced by manganese oxides which had soaked into the original structure. (Figure 4-3-6)

3) Distribution

The distribution of crusts is indicated by the coverage and the thickness of crust. The coverage of crust will be described in section 5), Results of FDC Survey. In this section 3), we will describe the thickness of crust.

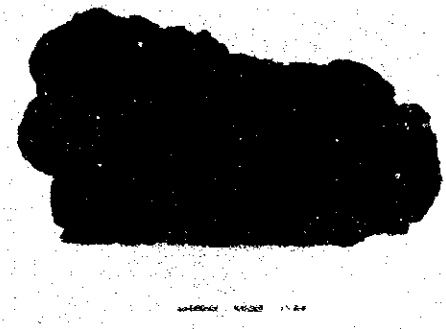

Botryoidal, 89SC06AD08

Botryoidal, 89SC06AD04

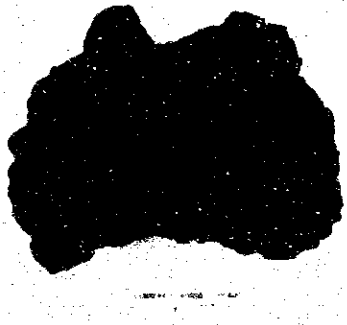

Botryoidal, 89SC06AD03

Botryoidal, 89SC06AD03

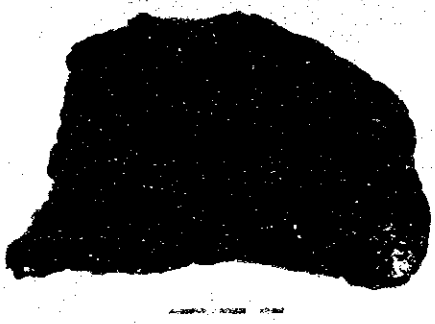

Rough, 89SC02AD05

Rough, 89SC05AD03

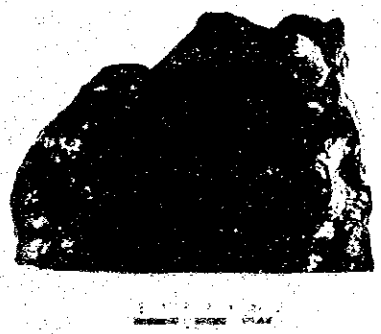

Smooth, 89SC04AD03

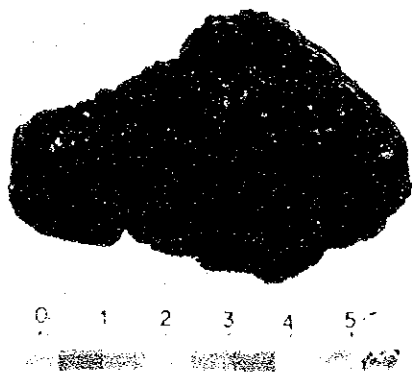

Smooth, 89SC06AD05

Figure 4-3-5 Characteristics of Cobalt Crust (Surface structure)

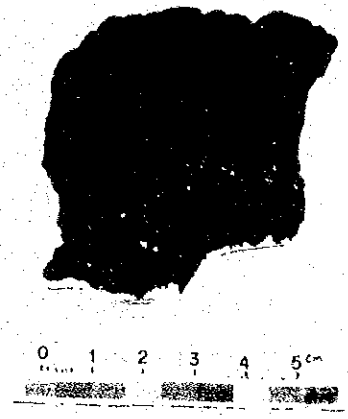

2 layered structure, 89SC06AD09

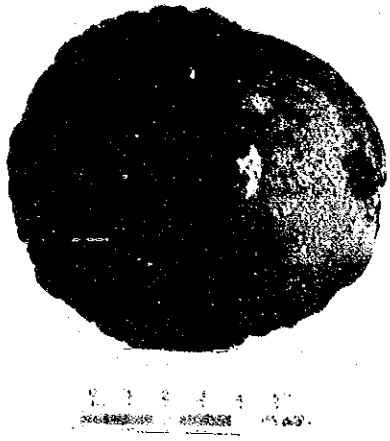

2 layered structure, 89SC01AD08

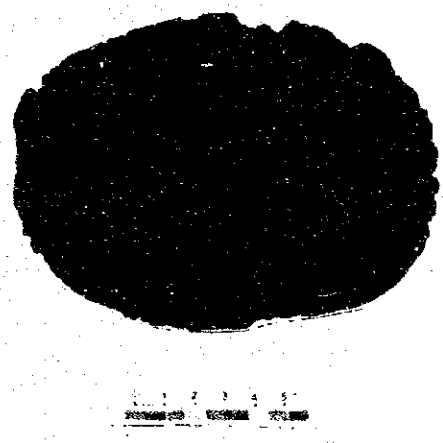

2 layered structure, 89SC01AD08

3 layered structure, 89SC06AD09

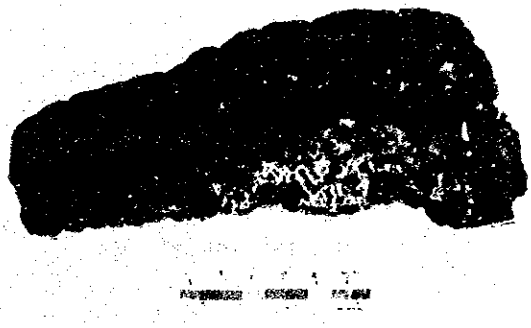

Texture of replaced limestone, 89SC02AD05

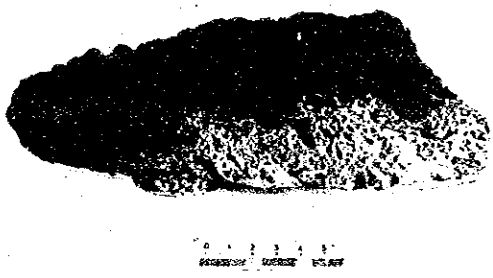

Cobalt crust shows texture of limestone in part, 89SC04AD09

Figure 4-3-6 Characteristics of Cobalt Crust (Section)

(1) The samples were detached and measured on board.

The results are classified according to elements of type, substrate, topography, depth, etc.. (Table 4-3-3 ~ Table 4-3-6 and Figure 4-3-7)

The following tendencies of the thickness of crusts are observed

① Excellent in depths below 1,500 m.

② Slab type has thick crust.

③ Excellent thickness is observed when the substrates are sedimentary rocks, pyroclastics, phosphorite and hyaloclastite, but basalt and limestone substrates have thin crusts.

④ Excellent thickness at summits and upper part of slopes.

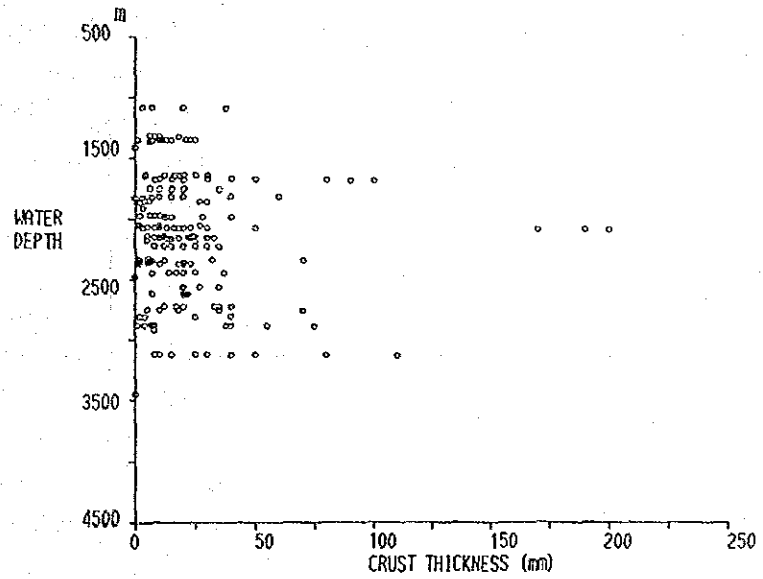

Figure 4-3-7 Thickness of Cobalt Crust and Water Depth

(2) Table 4-3-7 shows the distribution of crusts at each seamount. The characteristics of each seamount are as follows;

① Seamounts SC01 and SC02 have excellent thickness of crust, but seamount SC05, the summit of which is on the surface of the sea, has a thin cobalt crust.

② Grade of cobalt at seamounts SC02 and SC06 is excellent.

Table 4-3-3 Thickness of Cobalt Crust (by Type)

Type	n	Min. - Max. (mm)	Average (mm)
Crust type	79	2 ~ 70	19
Cobble type	11	1 ~100	28
Nodule type	12	1 ~ 50	18
Slab type	16	4 ~200	71
Pavement type	1	—	100

Table 4-3-4 Thickness of Cobalt Crust (by Substrate)

Substrate	n	Min. - Max. (mm)	Average (mm)
Basalt	12	1 ~ 70	15
Pyroclastics	20	5 ~100	27
Hyaloclastite	19	2 ~ 40	19
Limestone	20	2 ~ 37	13
Sedimentary rock	8	4 ~200	105
Phosphorite	2	13 ~ 38	26

Table 4-3-5 Thickness of Cobalt Crust (by Topography)

Topography	n	Min. - Max. (mm)	Average (mm)
Top flat	7	5 ~100	43
Vicinity of top	16	6 ~ 60	21
Upper part of Slope	44	1 ~200	32
Middle part of Slope	38	2 ~ 70	20
Lower part of Slope	15	1 ~110	28

Table 4-3-6 Thickness of Cobalt Crust (by Depth)

Depth (m)	n	Min. - Max. (mm)	Average (mm)
100 ~ 1,500	12	6 ~ 38	18
1,500 ~ 2,000	28	2 ~100	23
2,000 ~ 2,500	53	1 ~200	31
2,500 ~ 3,000	21	1 ~ 75	26
3,000 ~ 3,500	6	8 ~110	37

Table 4-3-7 Occurrences of Cobalt Crusts at Individual Seamounts (1)

Seamount	Occurrence
SC01 Depth of Summit 1,590 m 1,200 m	Depth Range : 1,280 - 2,880 m Crust type : Cobble is predominant. Slab type and Crust type are also well distributed. Substrate : Basalt and Hyaloclastite are predominant. Also, Limestone, Phosphorite, etc. Structure : Cobble type and Slab type are double layered. Thickness : 1 - 200 mm. Average of 7 samples is 35.4 mm. Grade : Co: 0.56%, Ni: 0.65%, Cu: 0.11%
SC02 Depth of Summit 1,040 m	Depth Range : 1,300 - 2,720 m Crust type : Crust type is predominant. Slab type, Cobble type and Nodule type are also recognised. Substrate : Basalt and Hyaloclastite are predominant. Also, Limestone, Phosphorite, etc.. Only Limestone is collected at the depth of less than 1,500 m. Structure : Single-layered or double-layered, also tri-layered. Thickness : 3-85 mm. Average of 7 samples is 21.7 mm. Grade : Co: 0.78%, Ni: 0.64%, Cu: 0.11%
SC03 Depth of Summit 1,140 m	Depth Range : 1,340 - 2,920 m Crust type : Crust type is predominant. Also, Nodule type and Cobble type are distributed. Substrate : Limestone is predominant. Also, Basalt, Hyaloclastite, Phosphorite, etc. Structure : Single-layered and double-layered, tri-layered too, Cobalt Crust breccia is noted in Limestone. Thickness : 1-80 mm. Average of 9 samples is 15.6 mm. Grade : Co: 0.54%, Ni: 0.56%, Cu: 0.13%

Table 4-3-7 Occurrences of Cobalt Crusts at Individual Seamounts (2)

Seamount	Occurrence
SC04 Depth of Summit 805 m	Depth Range : 890 - 3,230 m Crust type : Crust type is predominant. Also, Cobble, Slab and Nodule types. Substrate : Limestone is predominant. Also, Basalt, Hyaloclastite, Sandstone, Phosphorite etc. Only Limestone was collected at the depth of less than 1,700m. Structure : Mainly Single-layered. Thickness : 0-130 mm. Average of 8 samples is 19 mm. Grade : Co: 0.42%, Ni: 0.59%, Cu: 0.13%
SC05 Table Reef	Depth Range : 1,090 - 2,930 m Crust type : Mostly Coating type, development of crust is poor. Also, Cobble, Nodule and Slab types. Substrate : Limestone is predominant. also, Hyaloclastite, Phosphorite, etc. Only Limestone was collected at the depth of less than 1,200 m Structure : Single-layered. Thickness : 1-20 mm. Average of 8 samples is 6.5 mm. Grade : Co: 0.66%, Ni: 0.53%, Cu: 0.10%
SC06 Depth of Summit 1,130 m	Depth Range : 1,140 - 2,880 m Crust type : Crust type and slab type are distributed. Substrate : Basalt, Hyaloclastite are predominant with Limestone, Phosphorite etc. Structure : Double-layered in Crust type and Slab type. Thickness : 1-85 mm. Average of 9 samples is 18.9 mm. Grade : Co: 0.76%, Ni: 0.60%, Cu: 0.11%